Electronic Supplementary Materials (ESI)

Pillar[5]arene/albumin biosupramolecular systems for simultaneous native protein preservation and encapsulation of water-soluble substrate

Vildan Sultanaev,*[a] Luidmila Yakimova,*[a] Anastasia Nazarova,[a] Igor Sedov,[a] Olga Mostovaya,[a] Timur Mukhametzyanov,[a] Damir Davletshin,[b] Daria Takuntseva,[a] Elvina Gilyazova,[b] Emil Bulatov,[b] and Ivan Stoikov*[a]

[a] A.M. Butlerov Chemistry Institute of Kazan Federal University, 18 Kremlyovskaya Str., 420008 Kazan, Russia;

[b] *Institute of Fundamental Medicine and Biology, Kazan Federal University, 18 Kremlyovskaya Str., 420008 Kazan, Russia.*

Content

1. Synthesis S3

2. NMR, IR, ESI HRMS Spectra of pillar[5]arenes **4–6** S5

3. Graphs and Images Related to Biological Activity Studies S12

4. UV-vis, Fluorescence, Circular Dichroism, NMR Spectra, Data, and DLS Plots, Images Obtained by Computer Simulations S13

5. Supplemental References S30

1. Synthesis

4,8,14,18,23,26,28,31,32,35-Decakis-[(N-[2-dimethyl({ethoxycarbonyl[S-benzyl]methyl} aminocarbonylmethyl)ammonio]ethyl)aminocarbonylmethoxy]-pillar[5]arene decabromide (1) was prepared by a literature method.[S1]

4,8,14,18,23,26,28,31,32,35-Decakis-[(N-[2-dimethyl(ethoxycarbonylaminocarbonyl methyl)ammonio]ethyl)aminocarbonylmethoxy]-pillar[5]arene decabromide (2) and **4,8,14,18,23,26,28,31,32,35-Decakis-[(N-[2-dimethyl({ethoxycarbonylmethyl}amino carbonylmethyl)ammonio]ethyl)aminocarbonylmethoxy]-pillar[5]arene decabromide (3)** were prepared by a literature method.[S2]

*General Procedure for the synthesis of pillar[5]arenes **4–6.***

0.0185 mmol of the ester (**1–3**) was placed in a round–bottom flask equipped with a magnetic stirrer, a 100–fold molar excess of LiOH and a mixture of solvents THF:H_2O = 1:1 (4 ml) were added to it. The reaction mixture was stirred at room temperature for one hour, then cooled at 0–4°C for about 12 hours. After cooling, the solution was acidified with 2M HCl to pH = 6–7 and stirred again for about 15 minutes. Solvents were removed using a rotary evaporator under reduced pressure. The resulting powder was poured into acetone, the mixture was stirred for about 20 minutes, and the solvent was removed under reduced pressure. The obtained compounds were dried under reduced pressure over P_2O_5.

4,8,14,18,23,26,28,31,32,35-Decakis-[(*N*-[2-dimethyl({oxycarbonyl[*S*-benzyl]methyl} aminocarbonylmethyl)ammonio]ethyl)aminocarbonylmethoxy]-pillar[5]arene (4). Brown powder. Yield: 0.056 g (77%). M.P. = 86 ºC.

^{1}H NMR (DMSO–d_6, 400 MHz, 298 K): δ_H, ppm, J/Hz: 2.91–3.04 (m, 20H, CHC$\underline{H}_2$Ph), 3.05–3.12 (m, 20H, NHCH$_2$C$\underline{H}_2$N$^+$), 3.13 (s, 60H, N$^+$(C$\underline{H}_3$)$_2$), 3.69–3.85 (m, 40H, ArC$\underline{H}_2$Ar, NHC$\underline{H}_2$CH$_2$N$^+$), 4.04–4.14 (m, 40H, N$^+$C$\underline{H}_2$C(O), ArOC$\underline{H}_2$), 4.48–4.57 (m, 10H, C$\underline{H}$CH$_2$Ph), 6.85 (s, 10H, Ar$\underline{H}$), 7.07–7.27 (m, 50H, Ph$\underline{H}$), 7.78–7.83 (m, 10H, ArOCH$_2$C(O)N$\underline{H}$), 8.62–8.82 (m, 10H, C(O)N$\underline{H}$CH).

^{13}C NMR (D_2O, 100 MHz, 298 K): δ_C, ppm: 28.1, 37.6, 52.4, 60.7, 62.2, 69.6, 126.9, 128.6, 129.2, 137.9, 162.9, 167.5, 171.1, 177.1.

IR (ν/cm^{-1}): 1202 (C–O–C), 1540 (N–H), 1658 (C=O), 1738 (COO$^-$), 3279, 3381 (N–H).

MS (ESI): calculated [M+3H$^+$]$^{3+}$ *m/z* = 1315.6337, [M+2H$^+$+Li$^+$]$^{3+}$ *m/z* = 1317.6364, found [M+3H$^+$]$^{3+}$ *m/z* = 1315.6242, [M+2H$^+$+Li$^+$]$^{3+}$ *m/z* = 1317.6287.

El. anal. calcd for $C_{205}H_{260}N_{30}O_{50}$, %: C, 62.42; H, 6.64; N, 10.65. Found, %: C 61.75; H 6.56; N 10.01.

4,8,14,18,23,26,28,31,32,35-Decakis-[(*N*-[2-dimethyl({oxycarbonylmethyl}amino carbonylmethyl)ammonio]ethyl)aminocarbonylmethoxy]-pillar[5]arene (5). Hygroscopic dark

beige powder. Yield: 0.045 g (84 %).

^{1}H NMR (DMSO–d_6, 400 MHz, 298 K): δ_H, ppm, J/Hz: 3.22–3.31 (m, 20H, NHCH$_2$C$\underline{H}_2$N$^+$), 3.34 (s, 60H, N$^+$(C$\underline{H}_3$)$_2$), 3.81–3.94 (m, 40H, NHC$\underline{H}_2$CH$_2$N$^+$, ArC$\underline{H}_2$Ar), 4.14–4.22 (m, 20H, NHC$\underline{H}_2$C(O)), 4.35–4.51 (m, 40H, N$^+$C$\underline{H}_2$C(O), ArOC$\underline{H}_2$), 6.88 (s, 10H, Ar$\underline{H}$), 8.78–8.83 (m, 10H, ArOCH$_2$C(O)N$\underline{H}$), 9.49–9.54 (m, 10H, C(O)N$\underline{H}$CH).

^{13}C NMR (DMSO-d_6, 100 MHz, 298 K): δ_C, ppm: 28.9, 33.3, 35.5, 51.5, 55.9, 62.7, 63.3, 67.5, 114.9, 128.2, 148.9, 161.7, 163.9, 168.7, 169.2, 170.5.

IR (ν/cm^{-1}): 1205 (C–O–C), 1546 (N–H), 1631 (C=O), 1739 (COO$^-$), 3083, 3381 (N–H).

MS (ESI): calculated [M+4H$^+$+Li$^+$]$^{5+}$ m/z = 610.4895, found [M+4H$^+$+Li$^+$]$^{5+}$ m/z = 610.1834.

El. anal. calcd for $C_{135}H_{200}N_{30}O_{50}$, %: C, 53.28; H, 6.62; N, 13.81. Found, %: C 52.44; H 6.90; N 13.07.

4,8,14,18,23,26,28,31,32,35-Decakis-[(*N*-[2-dimethyl({oxycarbonyl[*S*-methyl]methyl} aminocarbonylmethyl)ammonio]ethyl)aminocarbonylmethoxy]-pillar[5]arene (6). Hygroscopic dark beige powder. Yield: 0.048 g (81%).

^{1}H NMR (DMSO–d_6, 400 MHz, 298 K): δ_H, ppm, J/Hz: 1.31 (d, 30H, NHCHC$\underline{H}_3$, $^3J_{HH}$=7.2 Hz), 3.22–3.30 (m, 20H, NHCH$_2$C$\underline{H}_2$N$^+$), 3.33 (s, 60H, N$^+$(C$\underline{H}_3$)$_2$), 3.50–3.91 (m, 40H, NHC$\underline{H}_2$CH$_2$N$^+$, ArC$\underline{H}_2$Ar), 4.11–4.27 (m, 10H, NHC$\underline{H}$CH$_3$), 4.32–4.49 (m, 40H, N$^+$C$\underline{H}_2$C(O), ArOC$\underline{H}_2$), 6.86 (s, 10H, Ar$\underline{H}$), 8.70–8.91 (m, 10H, ArOCH$_2$C(O)N$\underline{H}$), 9.46–9.55 (m, 10H, C(O)N$\underline{H}$CH).

^{13}C NMR (DMSO-d_6, 100 MHz, 298 K): δ_C, ppm: 16.0, 28.9, 33.4, 49.2, 52.6, 60.8, 62.9, 67.9, 115.8, 129.2, 149.4, 163.6, 168.2, 171.3, 176.1.

IR (ν/cm^{-1}): 1203 (C–O–C), 1545 (N–H), 1659 (C=O), 1725 (COO$^-$), 3066, 3380 (N–H).

MS (ESI): calculated [M+3H$^+$]$^{3+}$ m/z = 1061.8616, [M+2H$^+$+Li$^+$]$^{3+}$ m/z = 1063.5298, found [M+3H$^+$]$^{3+}$ m/z = 1061.8530, [M+2H$^+$+Li$^+$]$^{3+}$ m/z = 1063.5278.

El. anal. calcd for $C_{145}H_{220}N_{30}O_{50}$, %: C, 54.71; H, 6.97; N, 13.20. Found, %: C 53.81; H 7.43; N 12.73.

2. NMR, IR, ESI HRMS Spectra of pillar[5]arenes 4–6

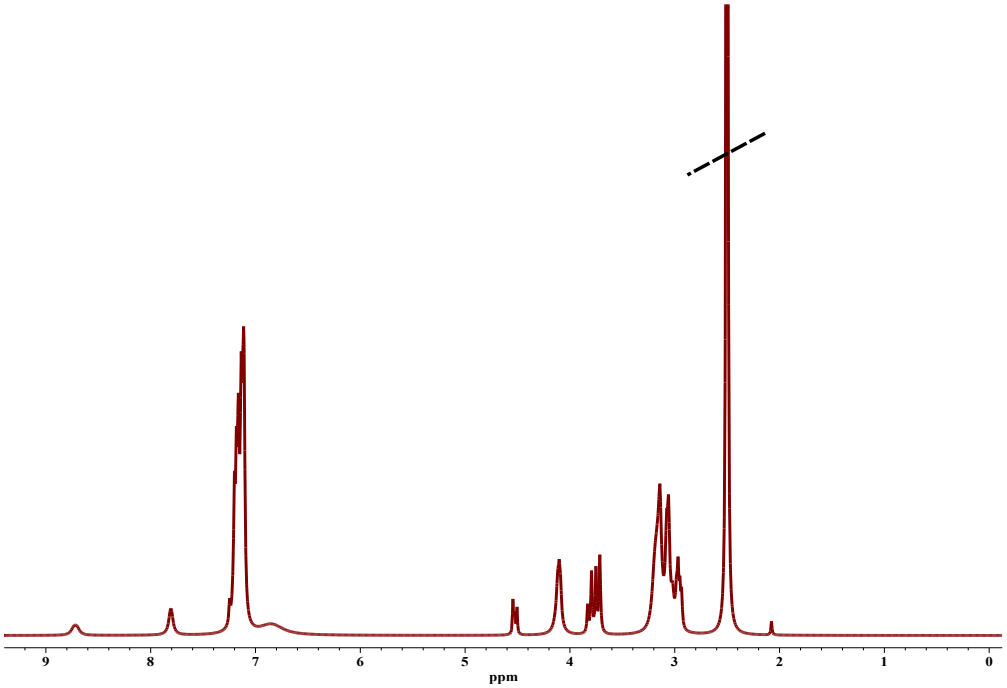

Figure S1. ^{1}H NMR spectrum of 4,8,14,18,23,26,28,31,32,35-Decakis-[(N-[2'-dimethyl({oxidocarbonyl[S-benzyl]methyl}aminocarbonylmethyl)ammonio]ethyl)aminocarbonyl methoxy]-pillar[5]arene (**4**), DMSO-d_6, 298 K, 400 MHz.

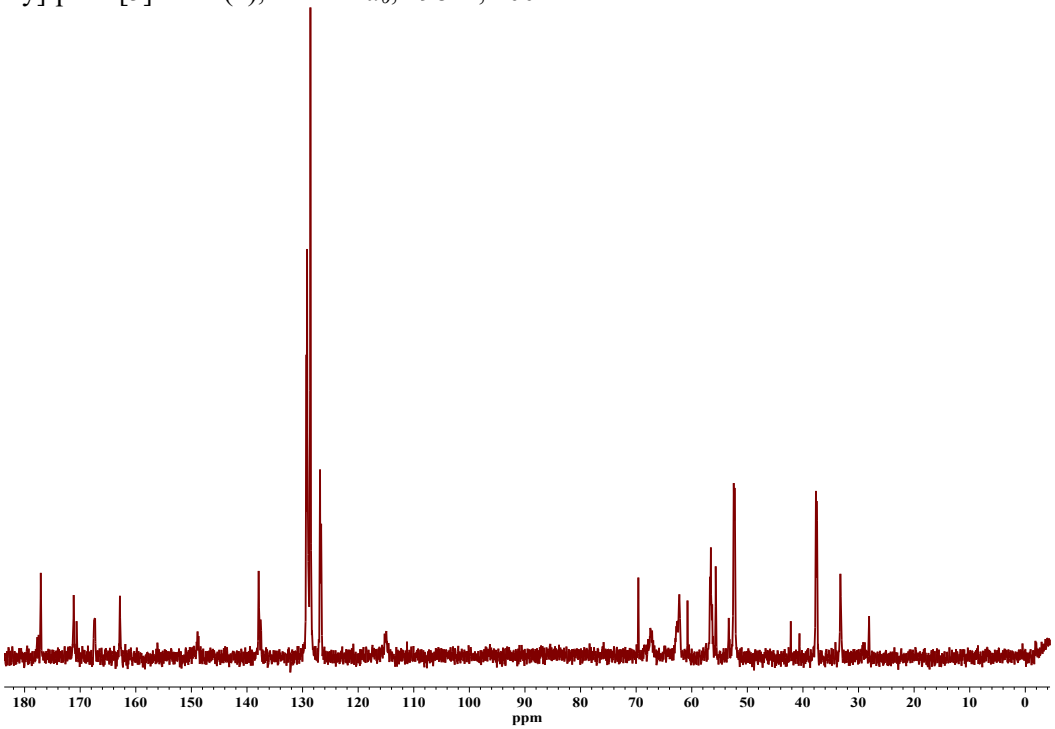

Figure S2. ^{13}C NMR spectrum of 4,8,14,18,23,26,28,31,32,35-Decakis-[(N-[2'-dimethyl({oxidocarbonyl[S-benzyl]methyl}aminocarbonylmethyl)ammonio]ethyl)amino carbonylmethoxy]-pillar[5]arene (**4**), DMSO-d_6, 298 K, 100 MHz.

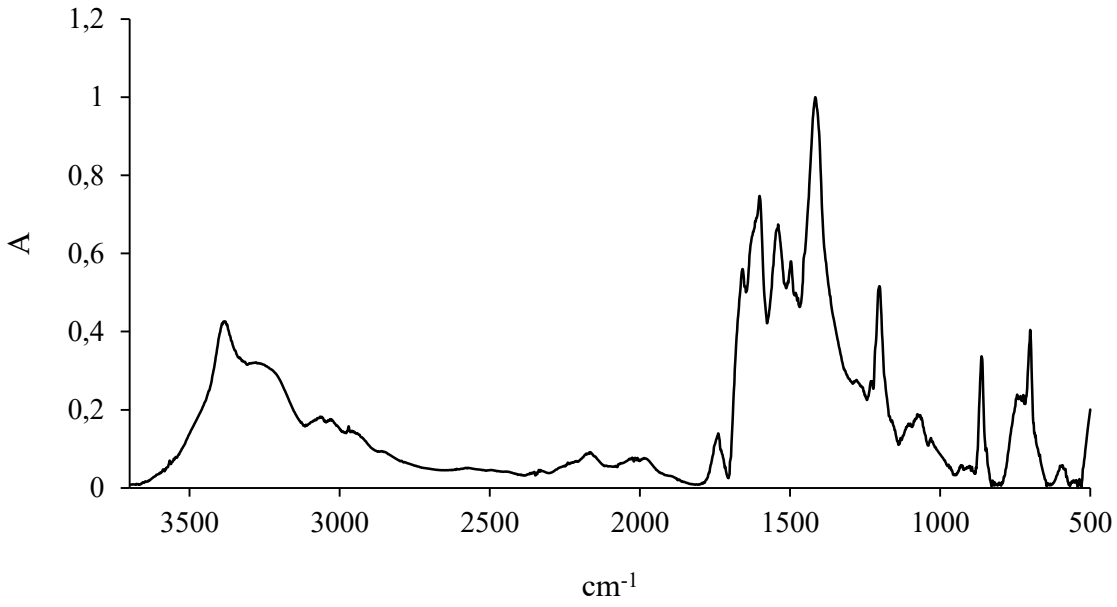

Figure. S3. IR spectrum of 4,8,14,18,23,26,28,31,32,35-Decakis-[(N-[2'-dimethyl({oxidocarbonyl[S-benzyl]methyl}aminocarbonylmethyl)ammonio]ethyl)aminocarbonylmethoxy]-pillar[5]arene (**4**).

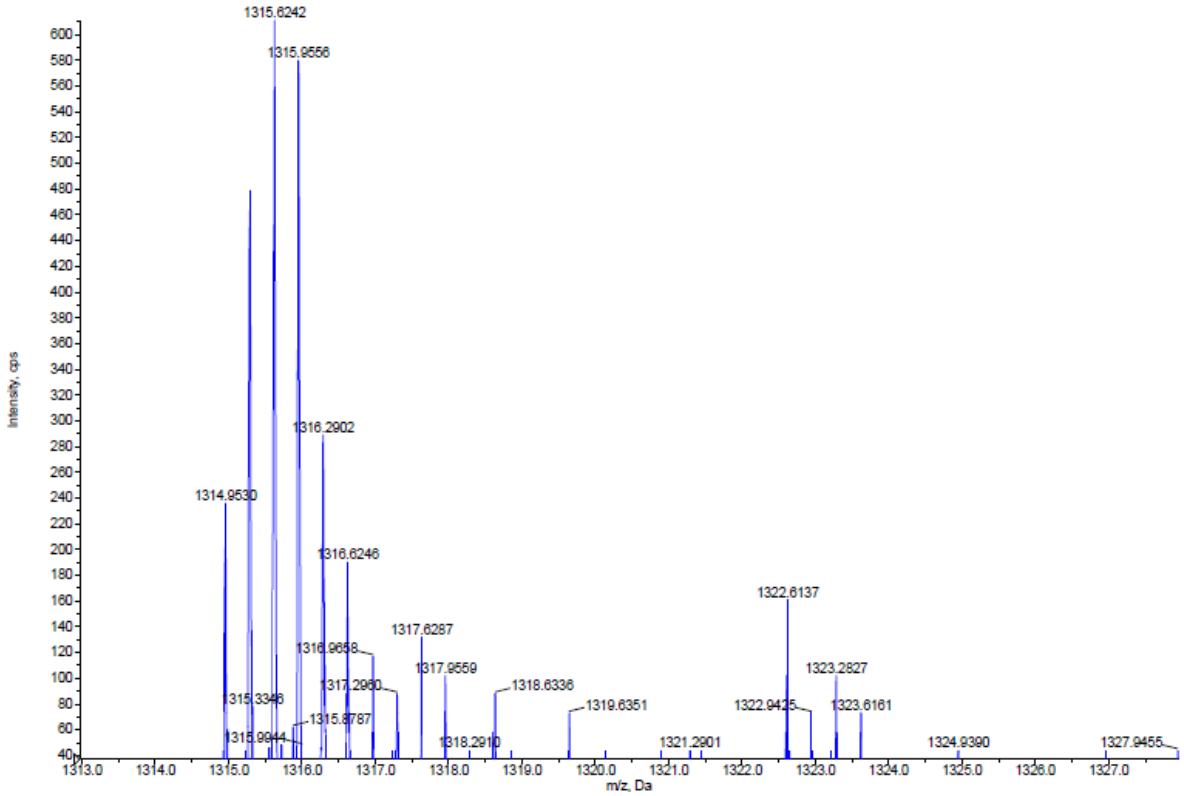

Figure. **S4**. Mass spectrum (ESI HRMS) of 4,8,14,18,23,26,28,31,32,35-Decakis-[(N-[2'-dimethyl({oxidocarbonyl[S-benzyl]methyl}aminocarbonylmethyl)ammonio]ethyl)aminocarbonyl methoxy]-pillar[5]arene (**4**).

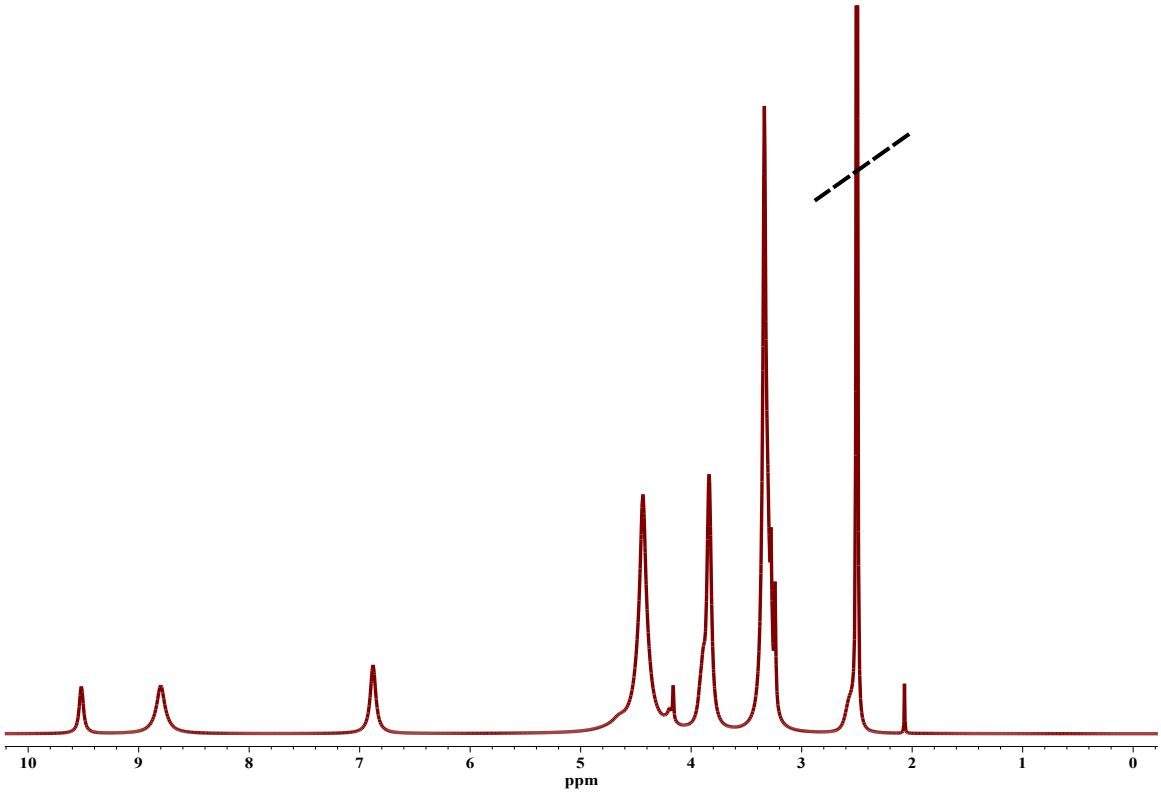

Figure. **S5.** ^{1}H NMR spectrum of 4,8,14,18,23,26,28,31,32,35-Decakis-[(*N*-[2'-dimethyl({oxidocarbonylmethyl}aminocarbonylmethyl)ammonio]ethyl)aminocarbonylmethoxy]-pillar[5]arene **(5)**, DMSO-d_6, 298 K, 400 MHz.

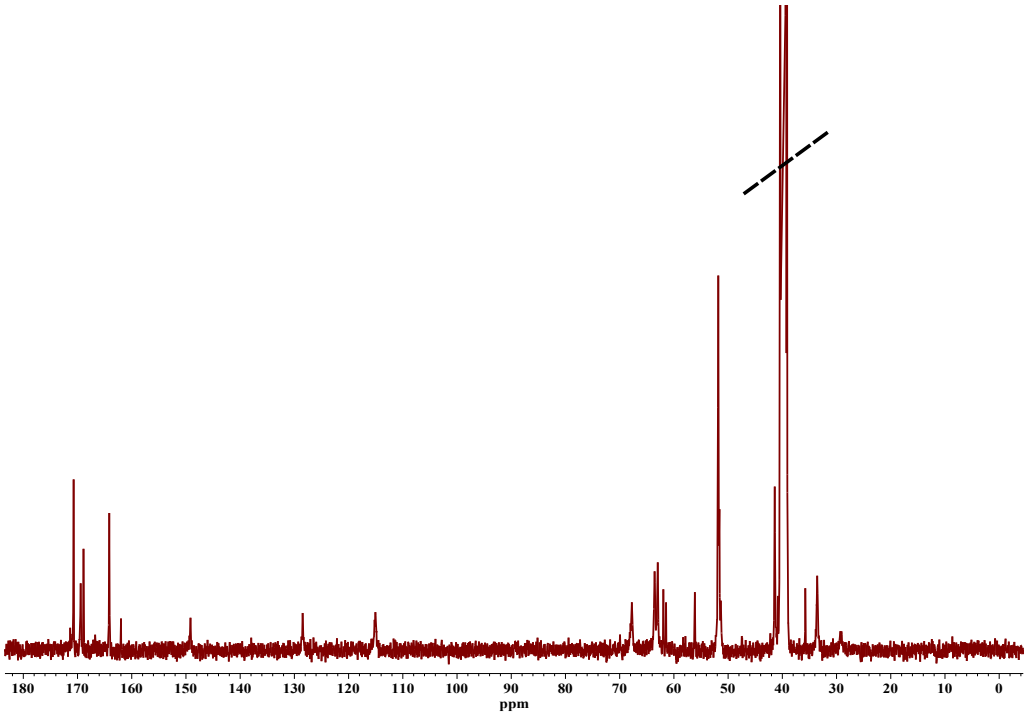

Figure. **S6**. ^{13}C NMR spectrum of 4,8,14,18,23,26,28,31,32,35-Decakis-[(*N*-[2'-dimethyl({oxidocarbonylmethyl}aminocarbonylmethyl)ammonio]ethyl)aminocarbonylmethoxy]-pillar[5]arene **(5)**, DMSO-d_6, 298 K, 100 MHz.

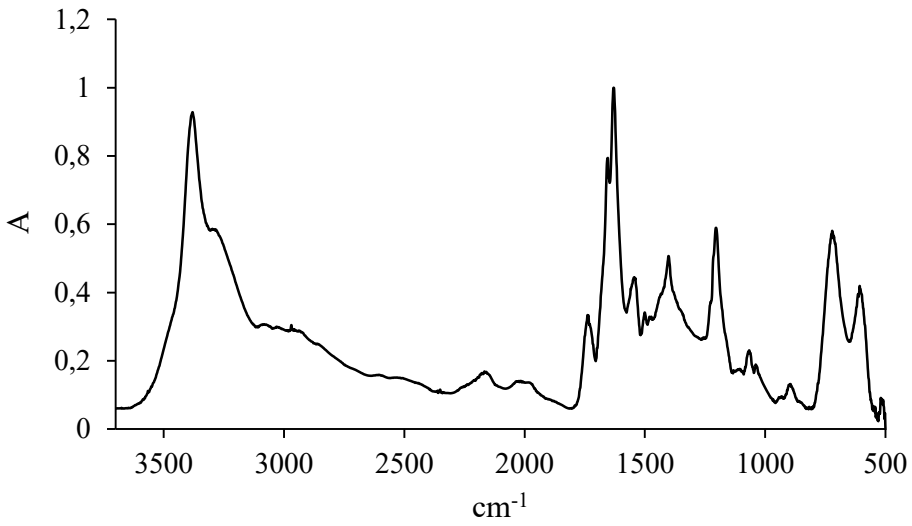

Figure. **S7**. IR spectrum of 4,8,14,18,23,26,28,31,32,35-Decakis-[(*N*-[2'-dimethyl({oxidocarbonylmethyl}aminocarbonylmethyl)ammonio]ethyl)aminocarbonylmethoxy] -pillar[5]arene **(5)**.

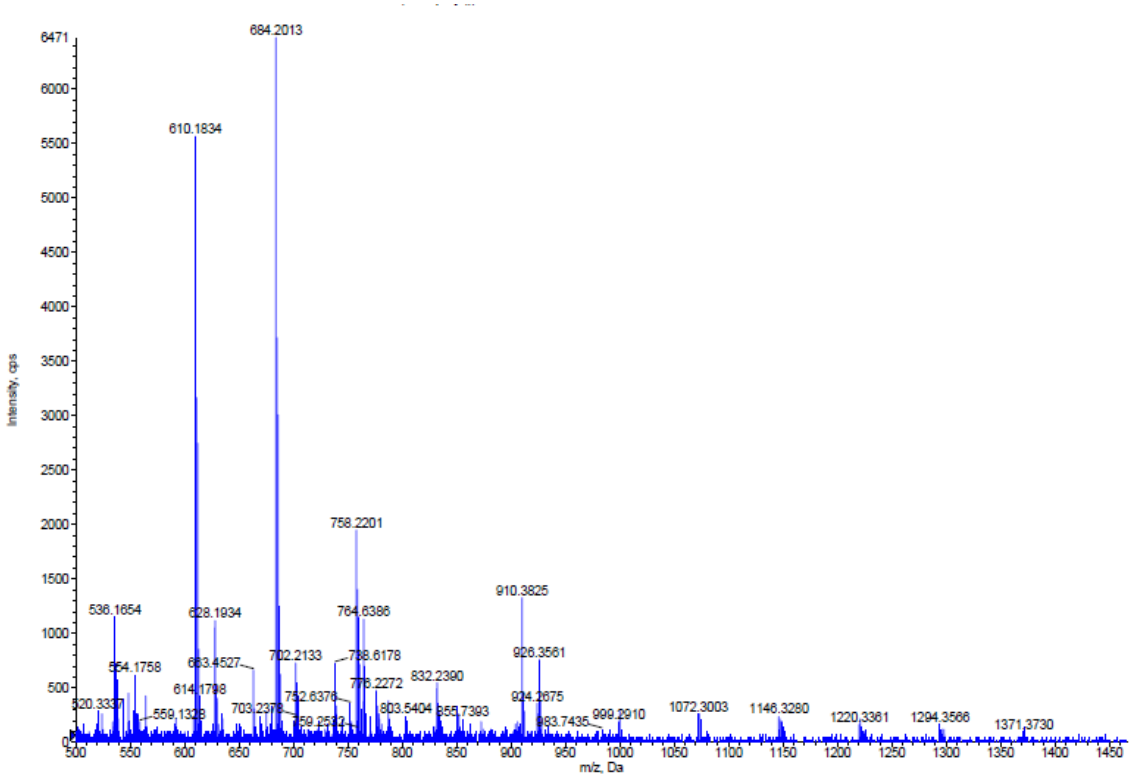

Figure. **S8**. Mass spectrum (ESI HRMS) of 4,8,14,18,23,26,28,31,32,35-Decakis-[(*N*-[2'-dimethyl({oxidocarbonylmethyl}aminocarbonylmethyl)ammonio]ethyl)aminocarbonylmethoxy]-pillar[5]arene **(5)**.

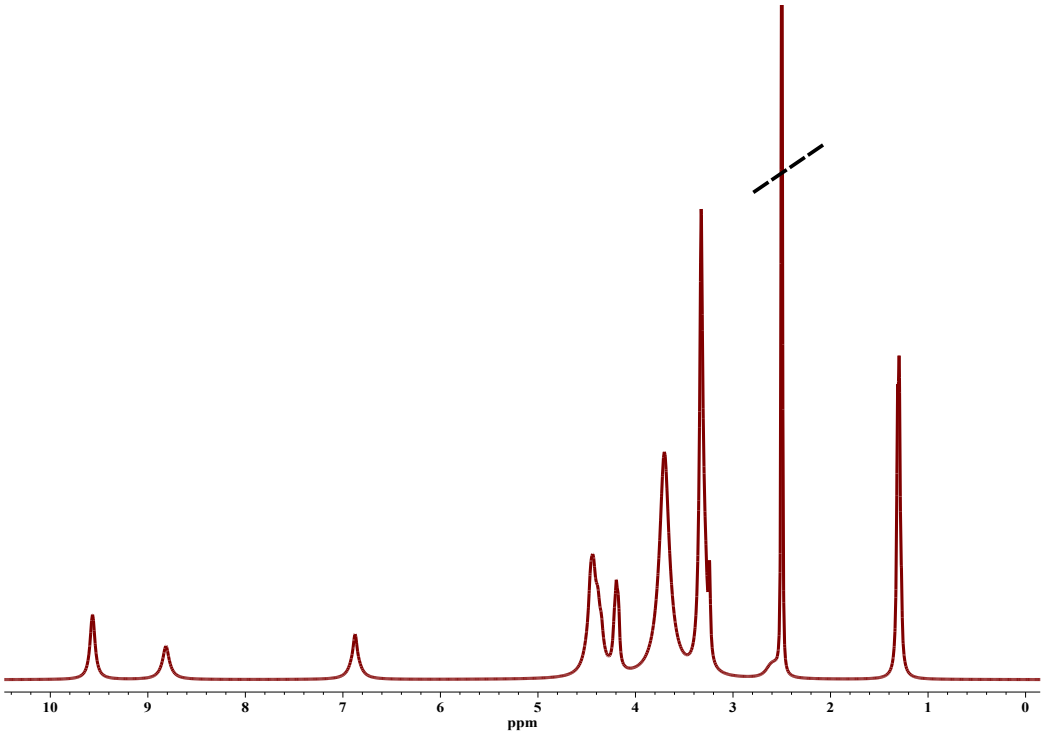

Figure. **S9.** ^{1}H NMR spectrum of 4,8,14,18,23,26,28,31,32,35-Decakis-[(*N*-[2'-dimethyl({oxidocarbonyl[*S*-methyl]methyl}aminocarbonylmethyl)ammonio]ethyl)aminocarbonyl methoxy]-pillar[5]arene **(6)**, DMSO-d_6, 298 K, 400 MHz.

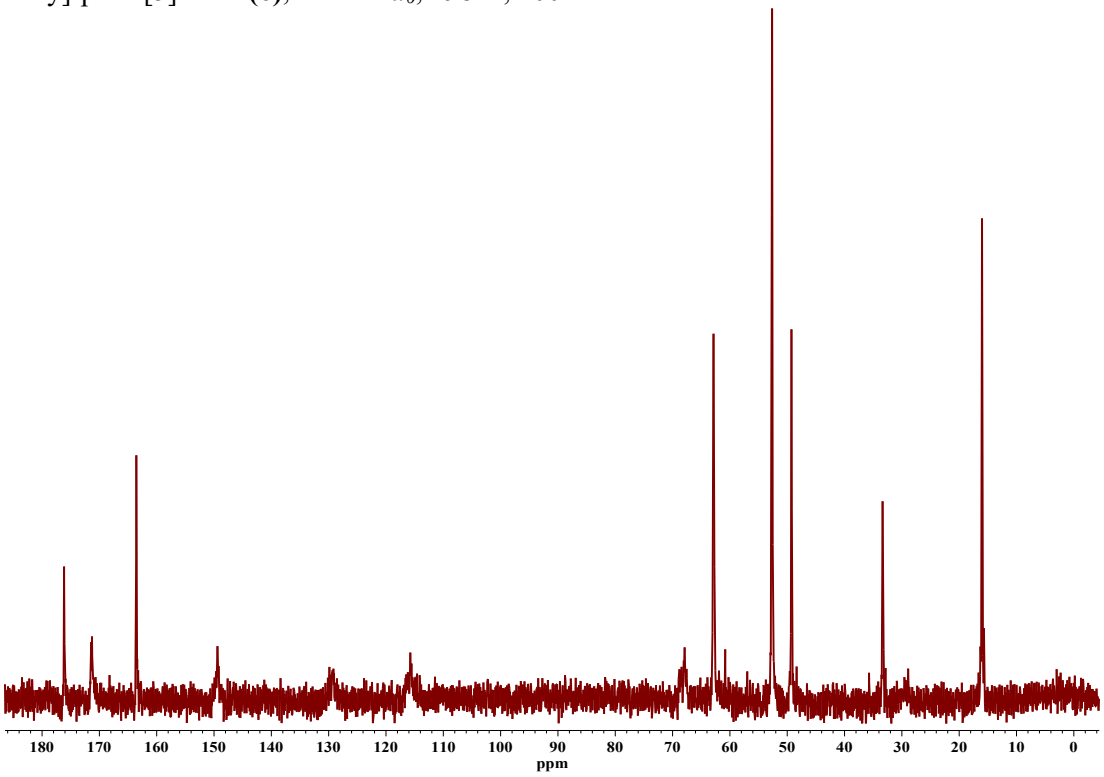

Figure. **S10**. ^{13}C NMR spectrum of 4,8,14,18,23,26,28,31,32,35-Decakis-[(*N*-[2'-dimethyl({oxidocarbonyl[*S*-methyl]methyl}aminocarbonylmethyl)ammonio]ethyl)aminocarbonyl methoxy]-pillar[5]arene **(6)**, DMSO-d_6, 298 K, 100 MHz.

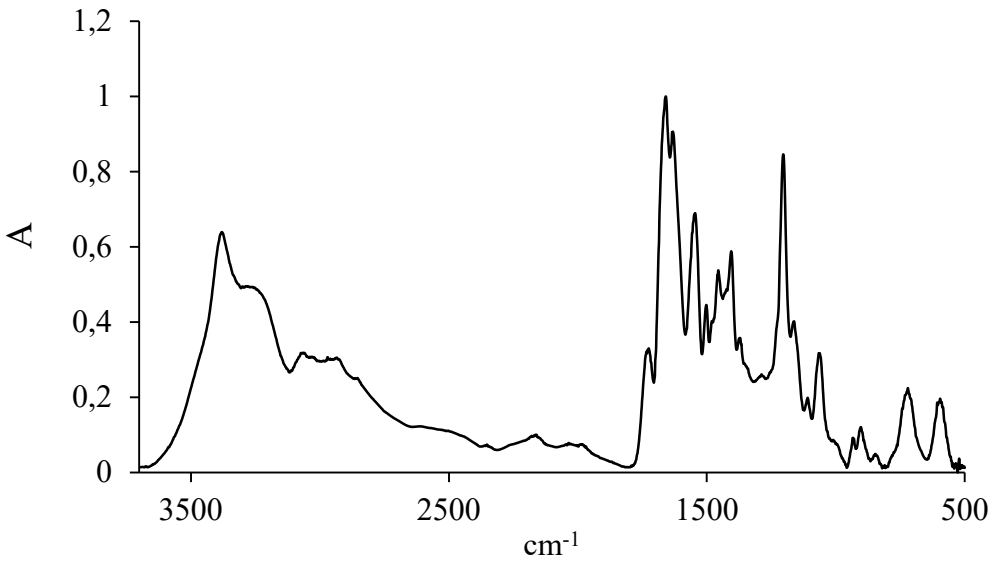

Figure. **S11**. IR spectrum of 4,8,14,18,23,26,28,31,32,35-Decakis-[(*N*-[2'-dimethyl({oxidocarbonyl[*S*-methyl]methyl}aminocarbonylmethyl)ammonio]ethyl)aminocarbonylmethoxy]-pillar[5]arene (**6**).

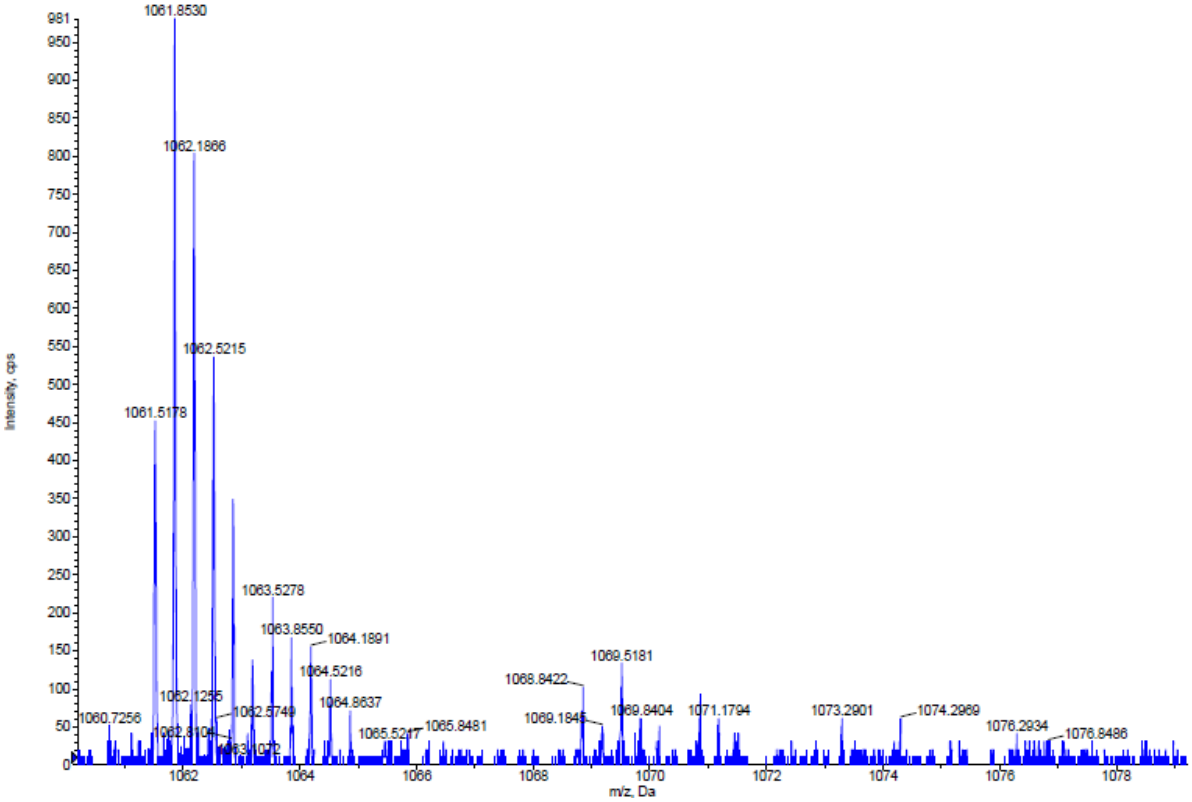

Figure. **S12**. Mass spectrum (ESI HRMS) of 4,8,14,18,23,26,28,31,32,35-Decakis-[(*N*-[2'-dimethyl({oxidocarbonyl[*S*-methyl]methyl}aminocarbonylmethyl)ammonio]ethyl)aminocarbonyl methoxy]-pillar[5]arene **(6)**.

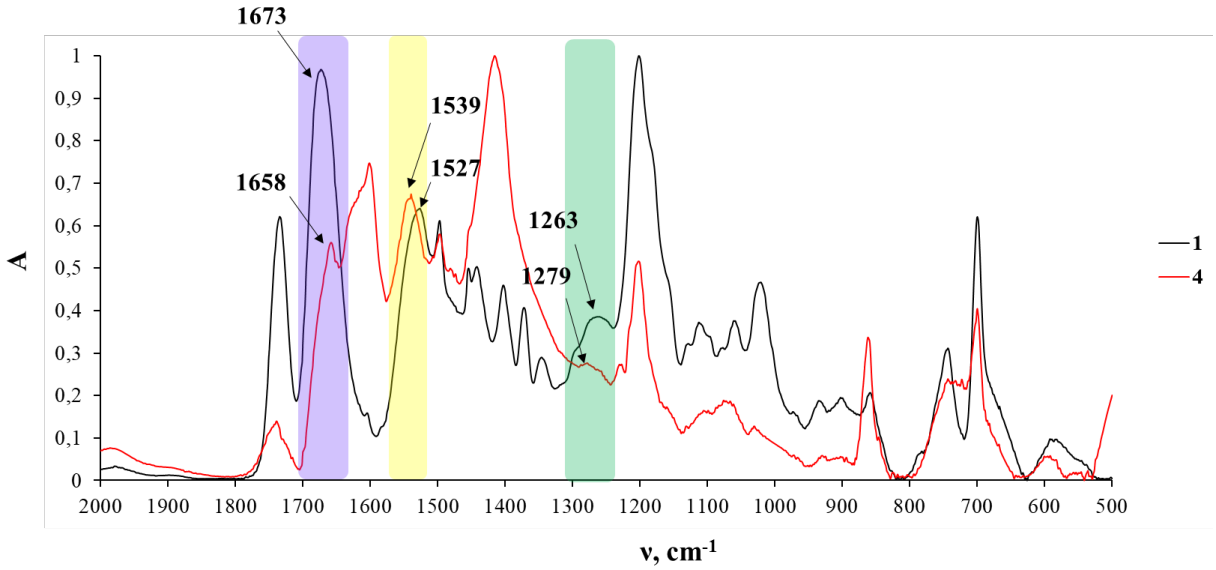

Figure. **S13**. Fragments of IR spectra of compounds **1** (black) and **4** (red).

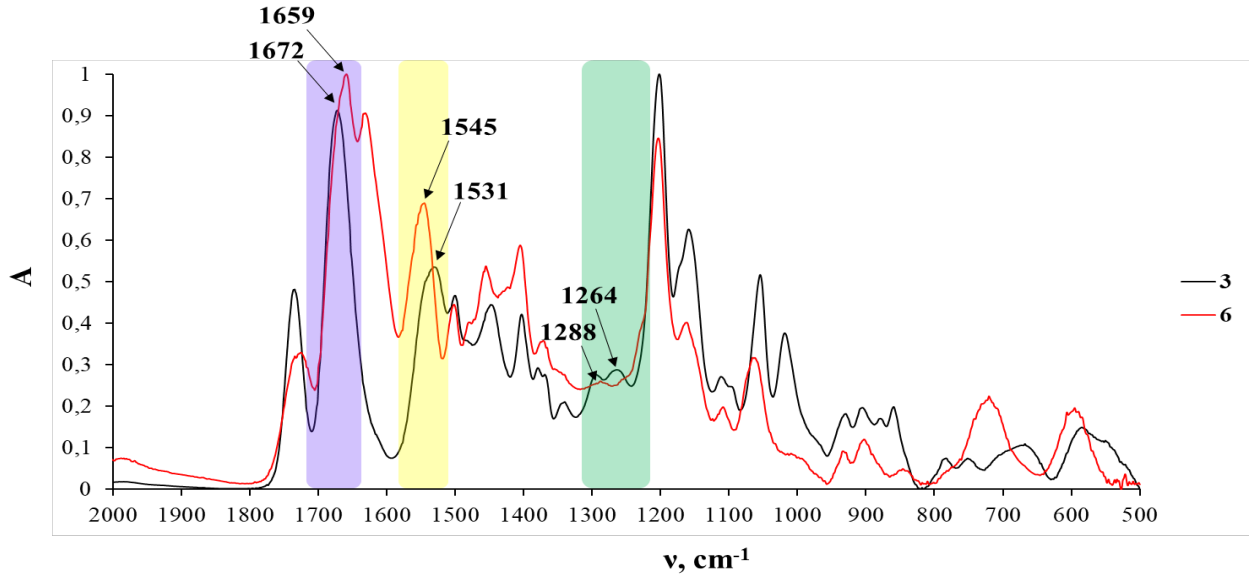

Figure. **S14.** Fragments of IR spectra of compounds 3 (black) and 6 (red).

3. Graphs and Images Related to Biological Activity Studies

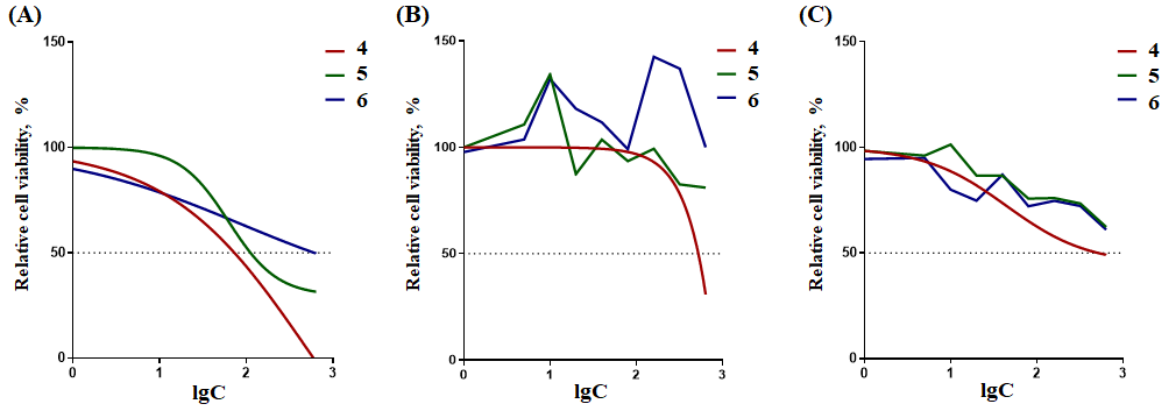

Figure S15. Graphs of cell viability of (A) MCF–7, (B) PC–3 and (C) HSF cell lines upon treatment with **4**, **5** and **6**.

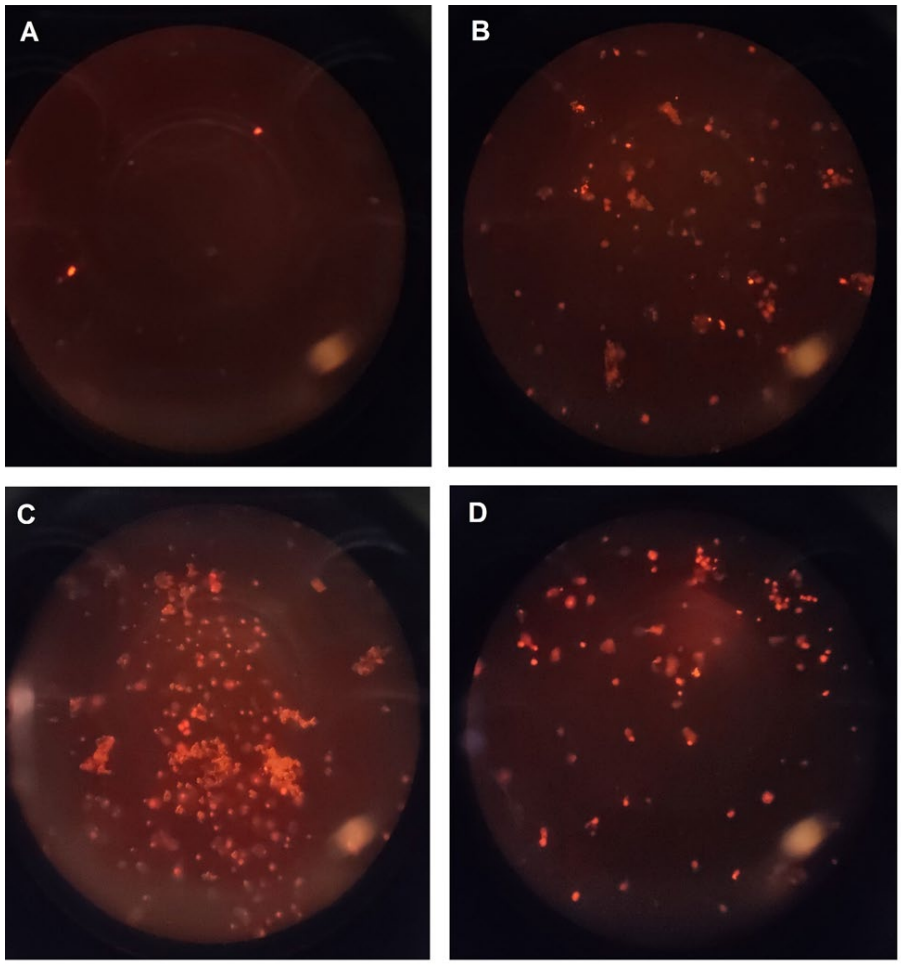

Figure S16. Fluorescent images demonstrating the effectiveness of PI transfection using macrocycle **4** at 10 μM (A), 20 μM (B), 40 μM (C) and 20 μM* (D).
* – cells were treated with PI and macrocycle **4** pre-mixed in a test tube

4. UV-vis, Fluorescence, Circular Dichroism, NMR Spectra, Data, and DLS Plots, Images Obtained by Computer Simulations

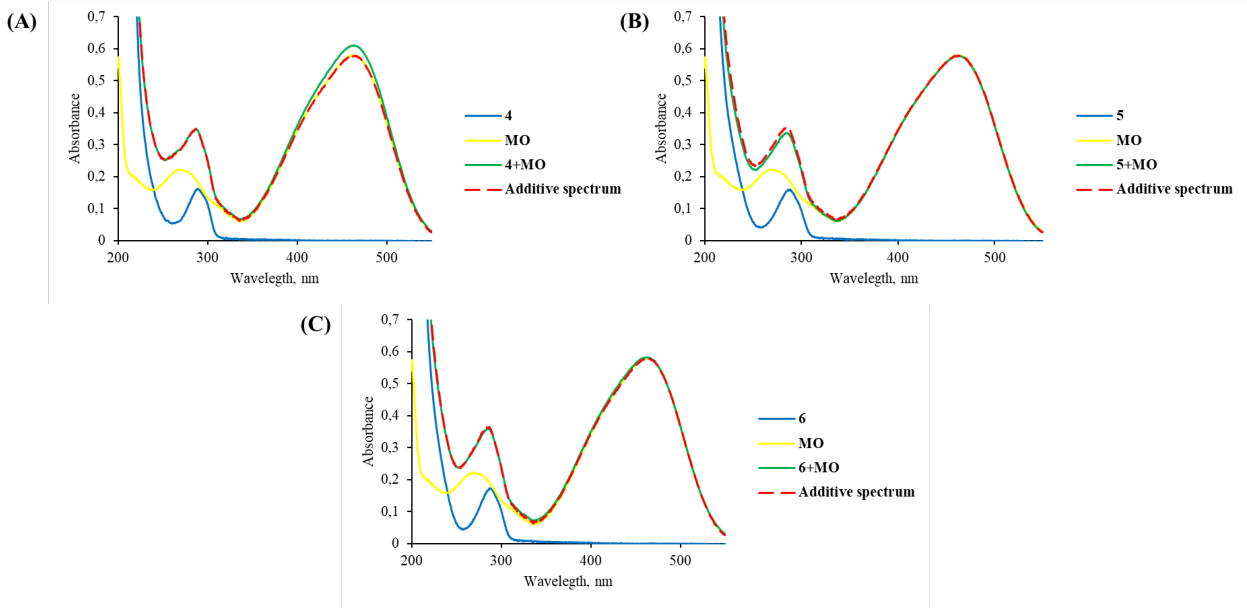

Figure S17. Electronic absorption spectra of **MO** (5×10^{-5} M) with macrocycles **4** (A), **5** (B) and **6** (C) in a 1:1 molar ratio in phosphate buffer at pH = 7.4.

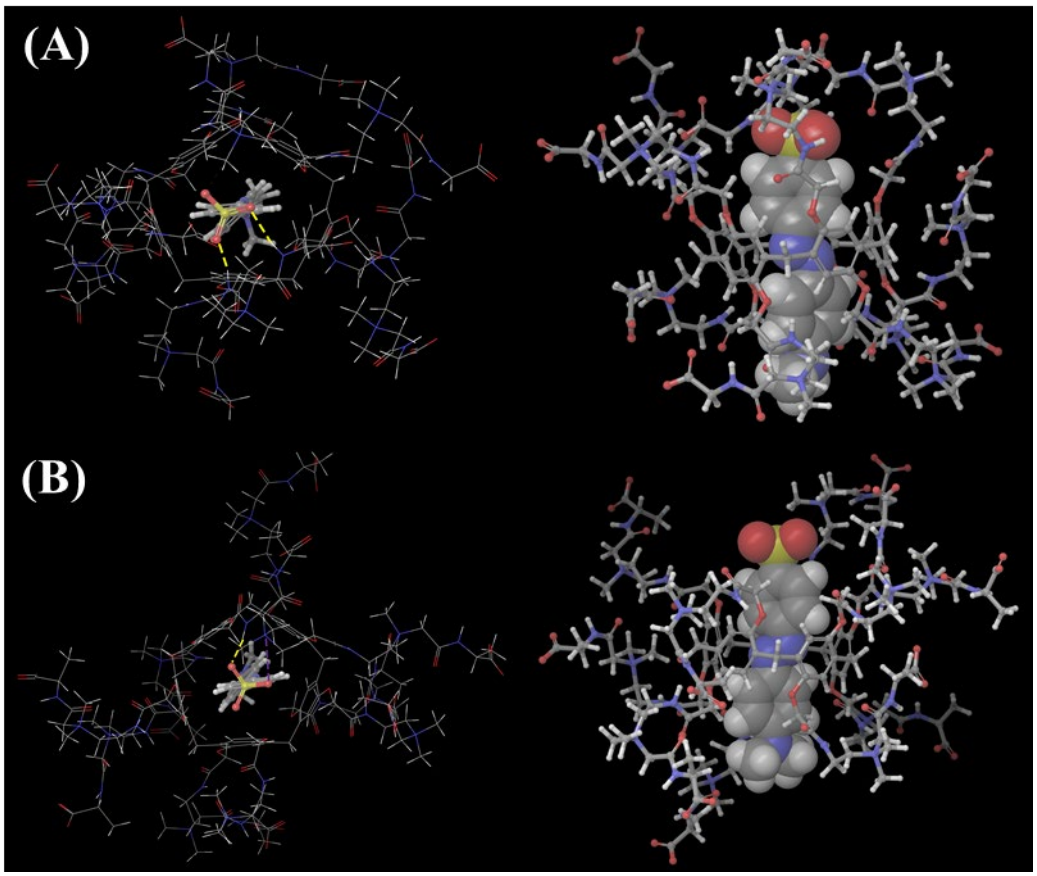

Figure S18. The snapshots of methyl orange complexes with macrocycle **5** (A) and **6** (B) from molecular dynamics simulations. Dashed lines represent hydrogen bonding (yellow) and electrostatic contacts between charged atoms (purple).

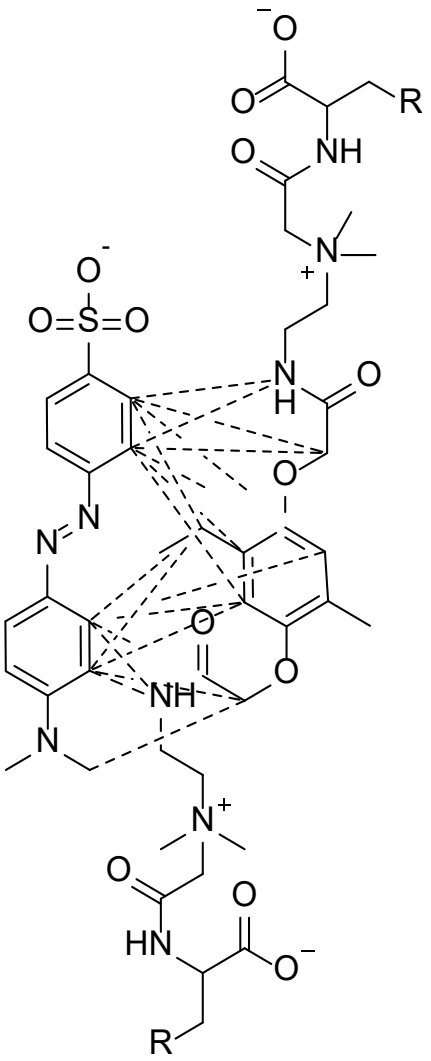

Figure S19. Close (< 5Å, dashed lines) contacts between pairs of hydrogen atoms in methyl orange and pillar[5]arenes that can be found in the majority of instantaneous configurations in the course of molecular dynamics runs.

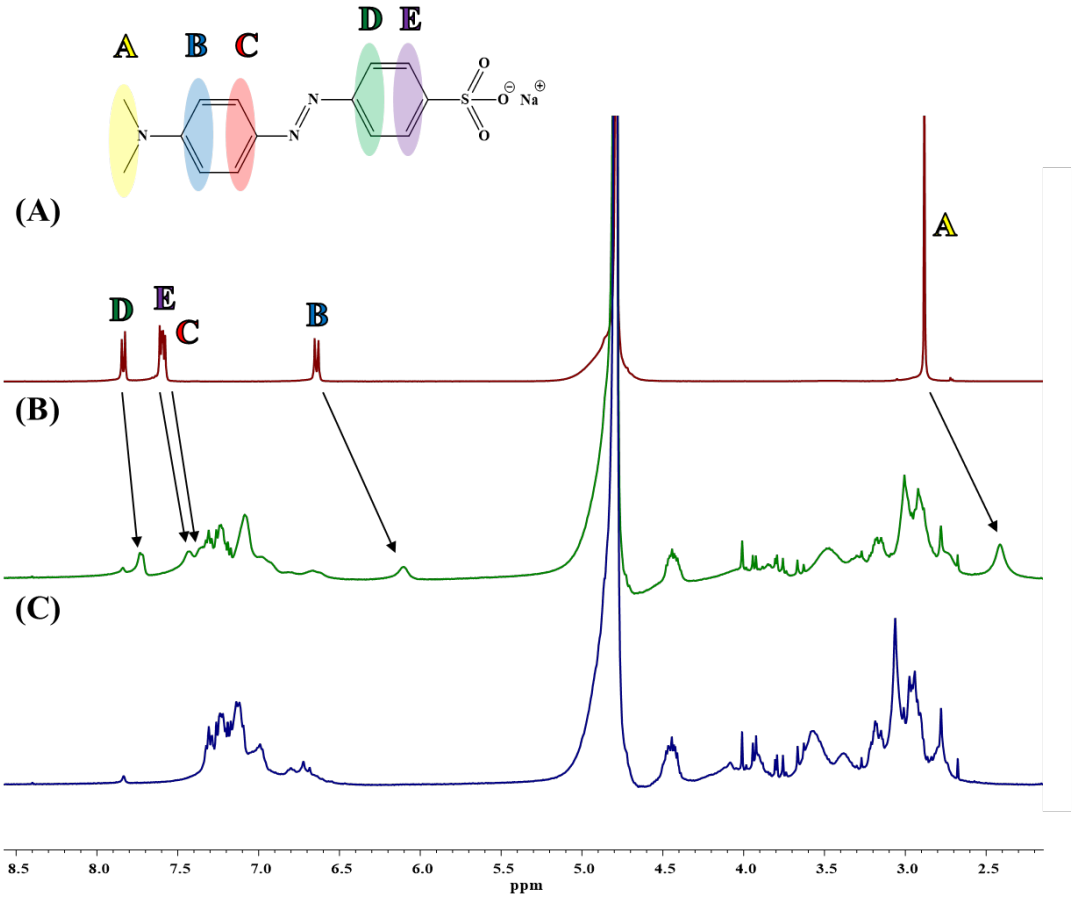

Figure S20. ^{1}H NMR spectra (D_2O, 298K, 400MHz): (A) **MO** (0.0112 mol/l); (B) **4** (0.0112 mol/l)–**MO** (0.0112 mol/l); (C) **4** (0.0112 mol/l).

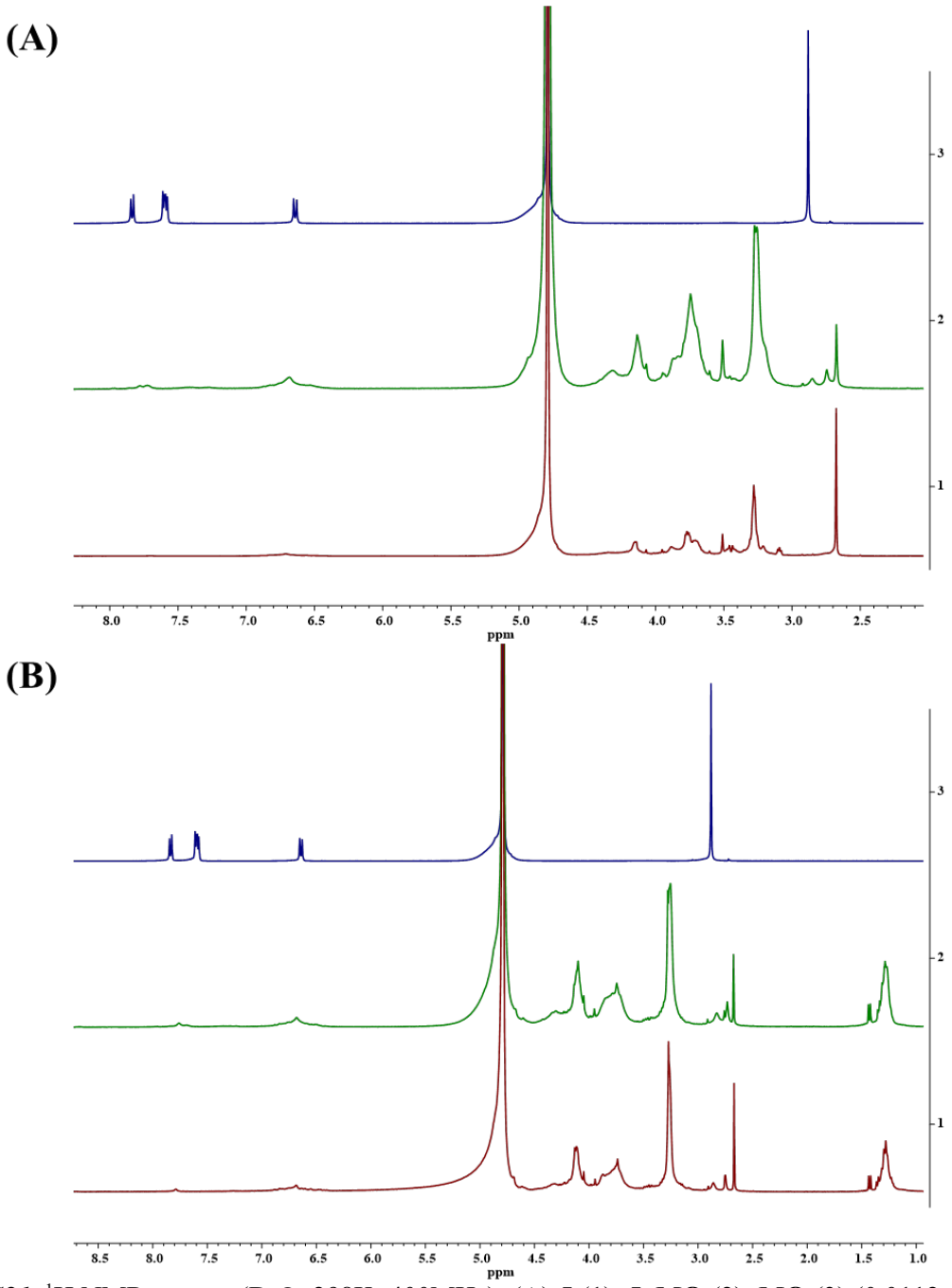

Figure S21. ^{1}H NMR spectra (D_2O, 298K, 400MHz): (A) **5** (1), **5–MO** (2), **MO** (3) (0.0112 mol/l); (B) **6** (1), **6–MO** (2), **MO** (3) (0.0112 mol/l);

Table S1. The aggregate sizes (hydrodynamic particle diameters d, nm), intensity distribution of particles formed as a result of self–assembly of compounds **4–6, MO** and their systems (1:1) in a phosphate buffer solution (pH=7.4), polydispersity index (PDI), zeta-potential (ζ).

System	PDI	d, nm	ζ, mV
4	0.30±0.02	261±5	-8±2
5	0.57±0.01	617±3	-13±1
6	0.66±0.23	514±186	-14±1
MO	0.34±0.03	259±11	-5±2
4+MO	0.35±0.07	272±42	-13±1
5+MO	0.66±0.03	707±116	-4±1
6+MO	0.61±0.10	845±105	-12±2

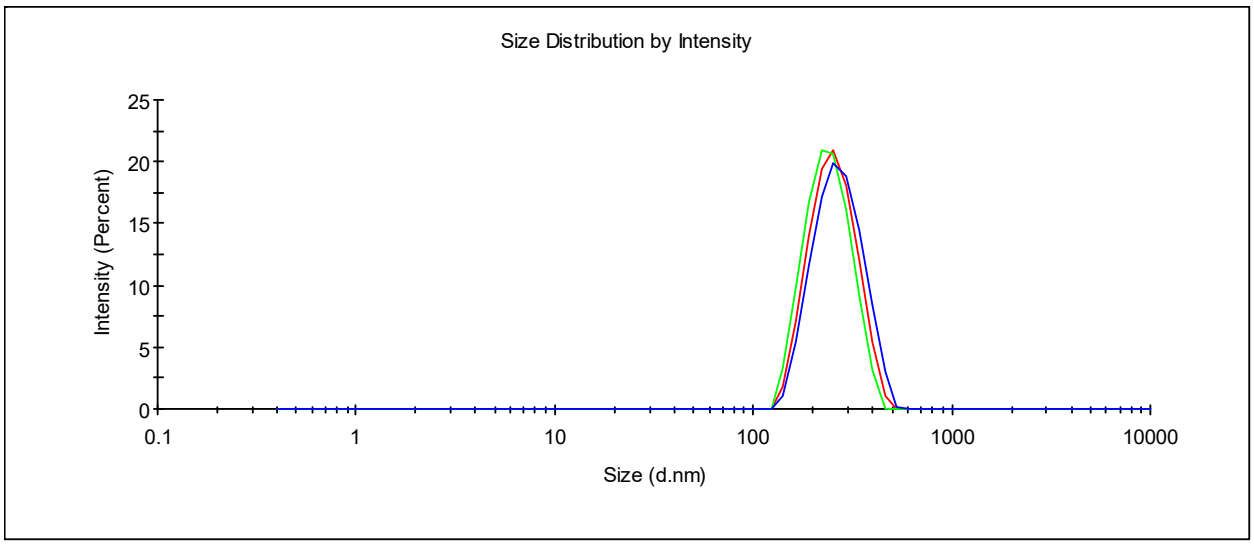

Figure S22. Size distribution of aggregates formed by macrocycle **4** in a phosphate buffer solution (pH = 7.4) (1×10^{-4} M).

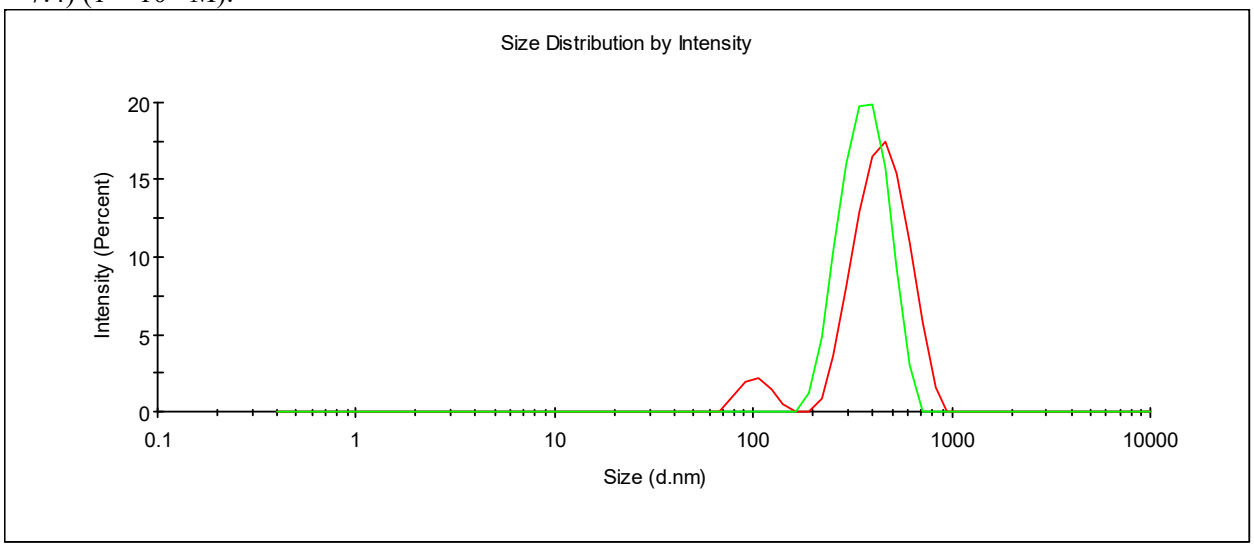

Figure S23. Size distribution of aggregates formed by macrocycle **5** in a phosphate buffer solution (pH = 7.4) (1×10^{-4} M).

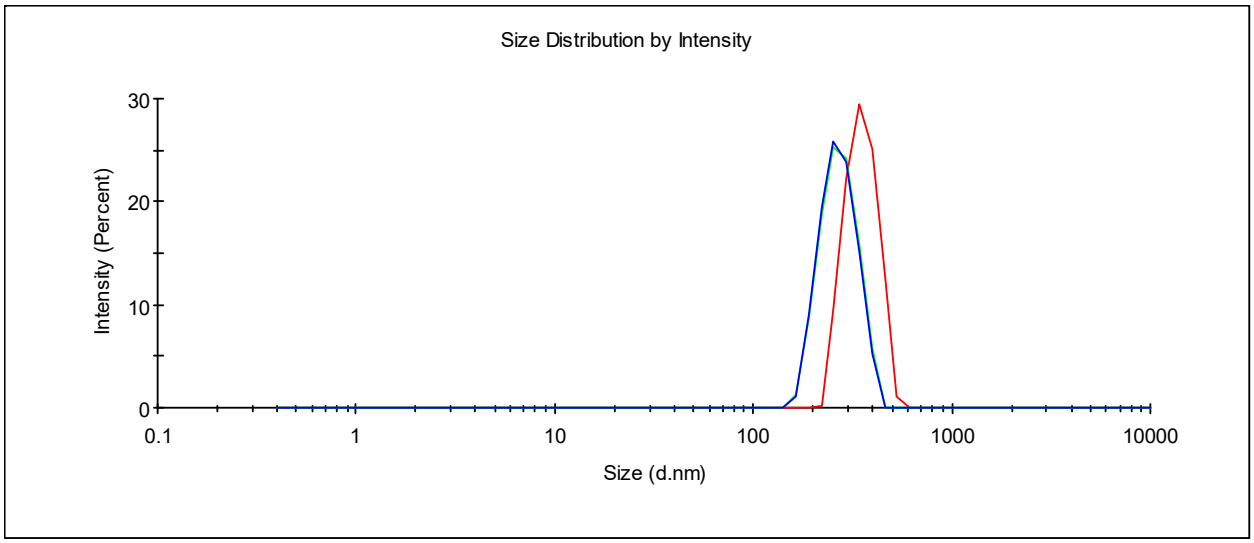

Figure S24. Size distribution of aggregates formed by macrocycle **6** in a phosphate buffer solution (pH = 7.4) (1×10^{-4} M).

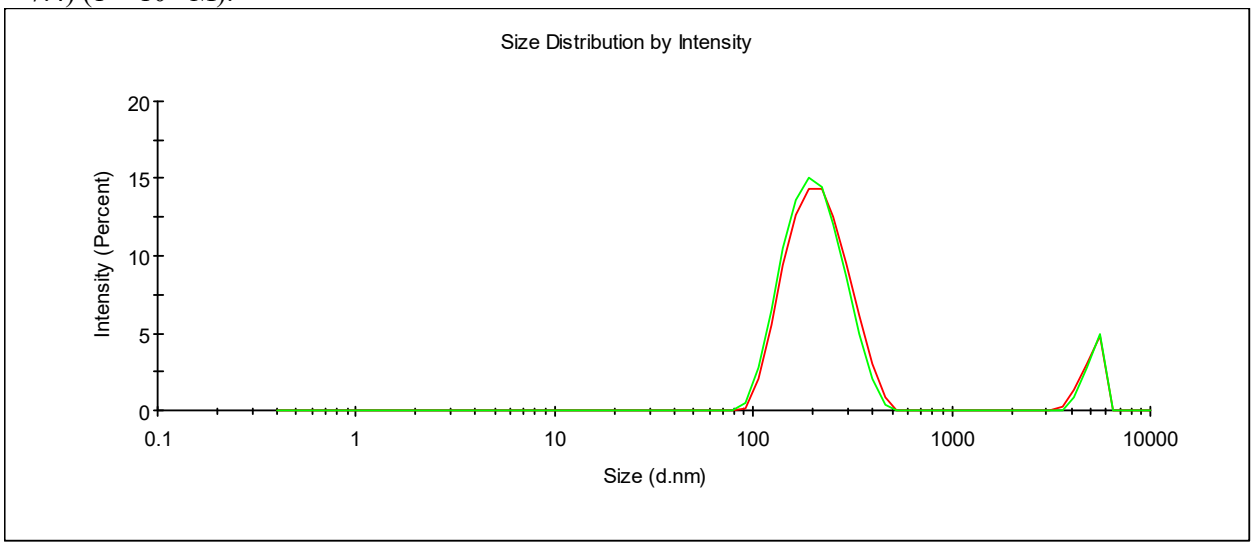

Figure S25. Size distribution of aggregates formed by macrocycle **MO** in a phosphate buffer solution (pH = 7.4) (1×10^{-4} M).

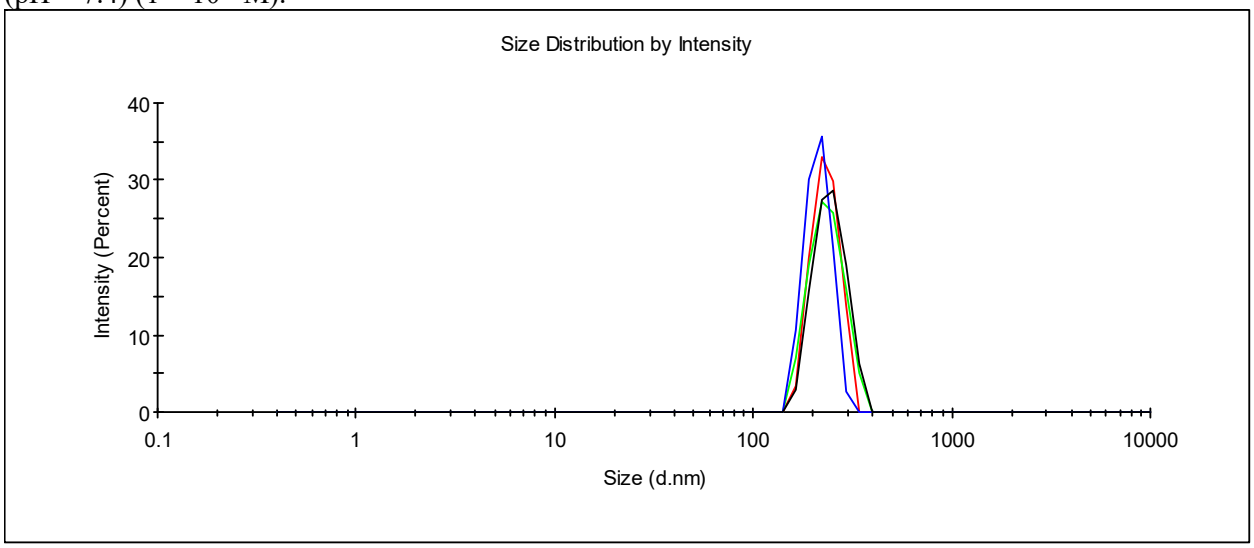

Figure S26. Size distribution of aggregates formed by **4**–**MO** in a phosphate buffer solution (pH = 7.4) (1×10^{-4} M).

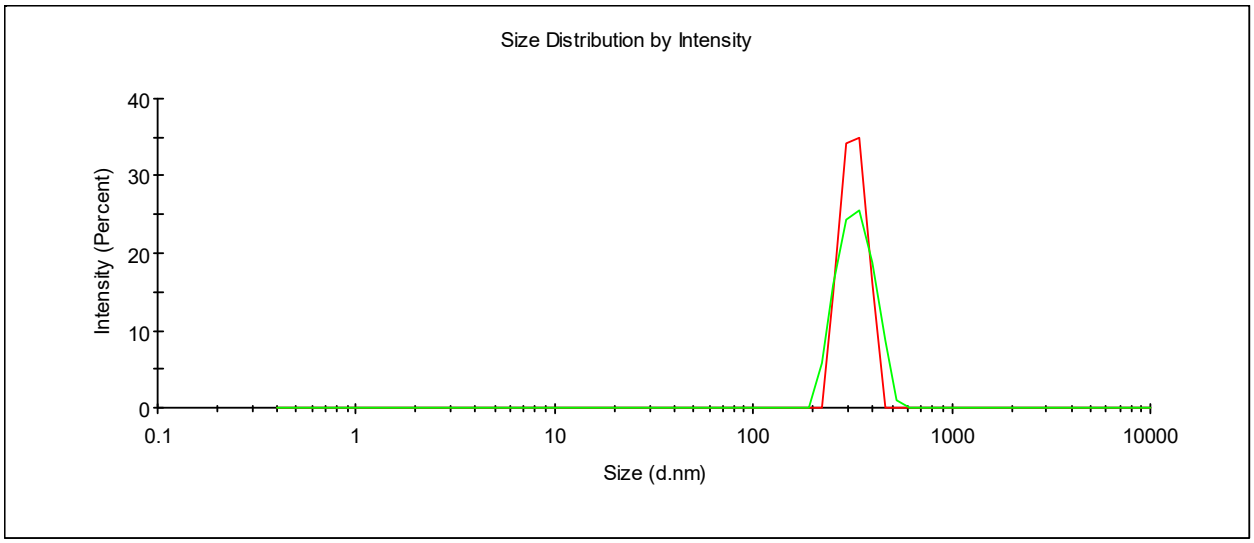

Figure S27. Size distribution of aggregates formed by **5**–**MO** in a phosphate buffer solution (pH = 7.4) (1×10^{-4} M).

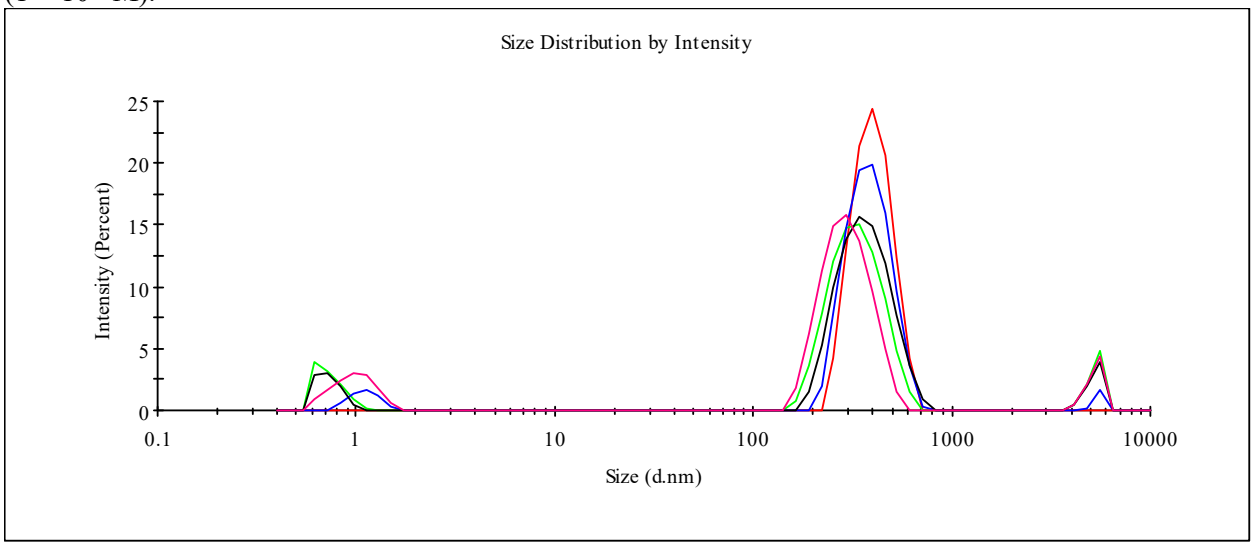

Figure S28. Size distribution of aggregates formed by **6**–**MO** in a phosphate buffer solution (pH = 7.4) (1×10^{-4} M).

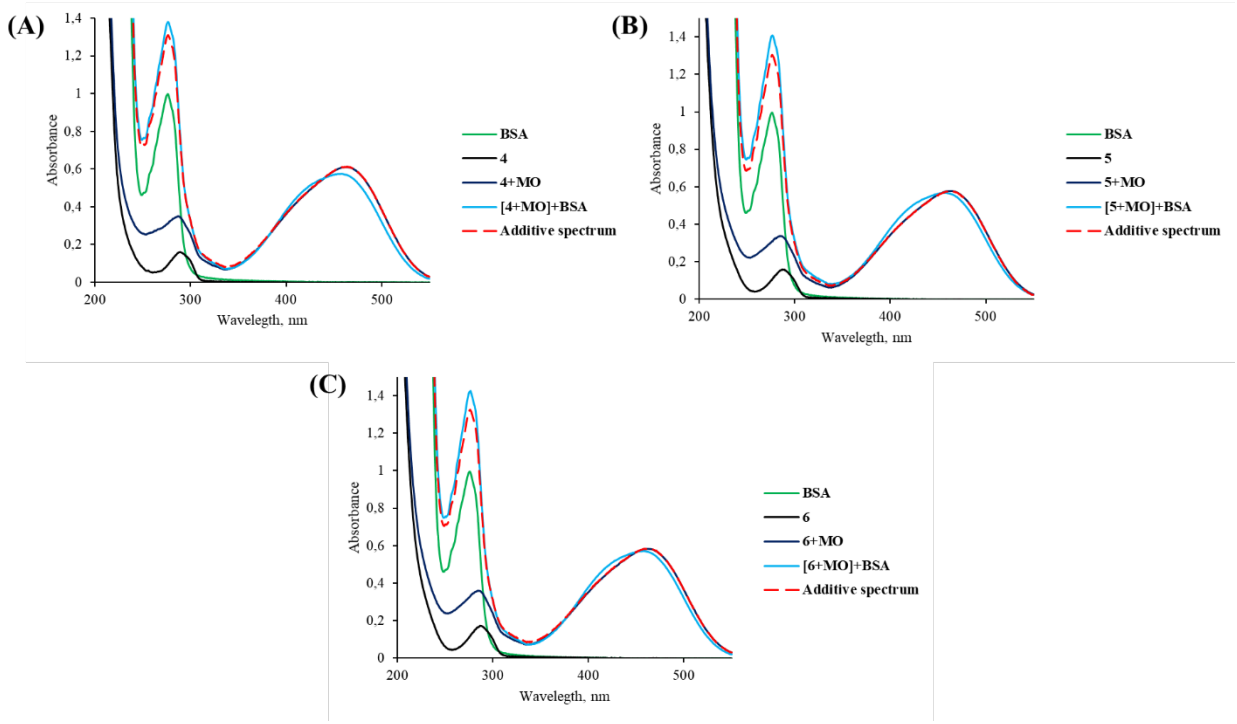

Figure S29. Electronic absorption spectra of BSA, **MO**, macrocycles (A) **4**; (B) **5**; (C) **6**, and mixtures of them in equimolar ratios in phosphate buffer at pH = 7.4 (C = 5 × 10^{-5} M).

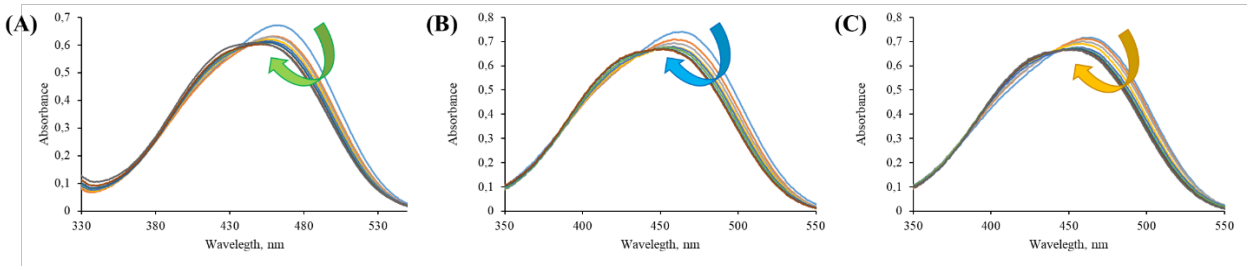

Figure S30. UV–vis spectra of triple mixtures of pillar[5]arenes **4** (A), **5** (B) and **6** (C) with **MO** (3 × 10^{-5} M) and BSA (9 × 10^{-6} – 7.5 × 10^{-5} M) in phosphate buffer solution at pH = 7.4. Arrows mean hypochromic effect and a blue shift with increasing concentration of protein.

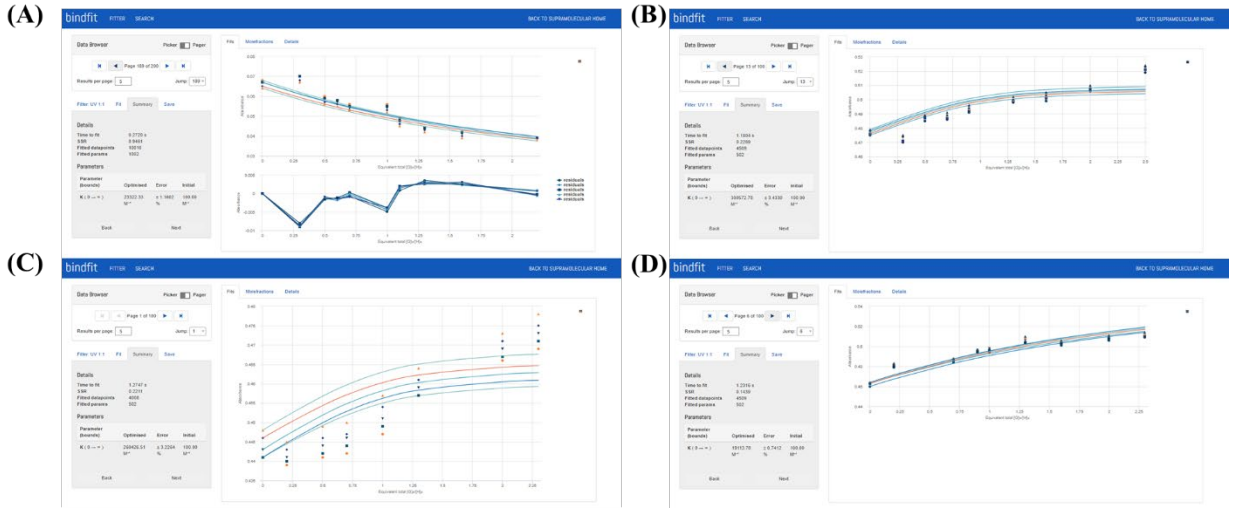

Figure S31. Bindfit screenshots taken from the summary window of the website supramolecular.org. This screenshots shows the raw data for UV–vis titration of (A) **MO**+BSA, (B) [**4–MO**]+BSA, (C) [**5–MO**]+BSA, and (D) [**6–MO**]+BSA in phosphate buffer at pH = 7.4, the data fitted to 1:1 binding model.

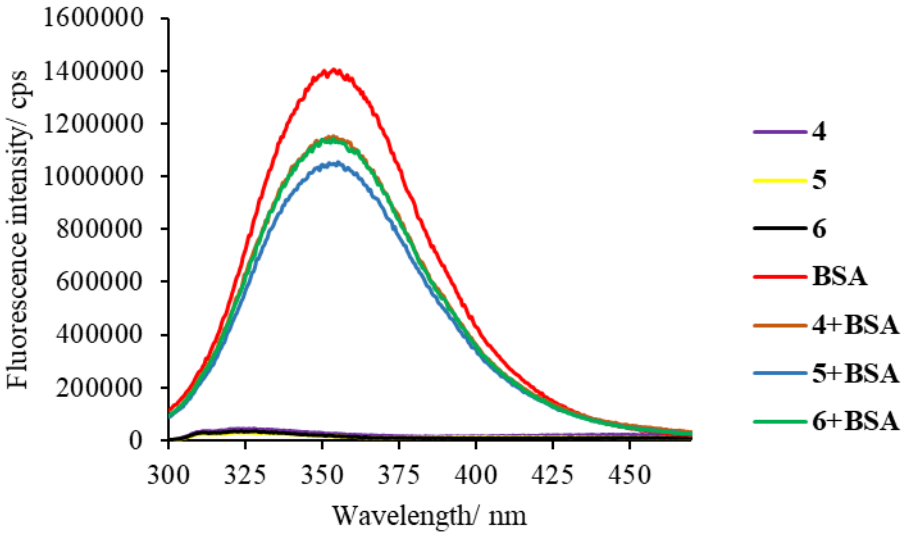

Figure S32. Fluorescence spectra of BSA (5×10^{-6} M) in the presence of pillar[5]arenes **4–6** (5×10^{-5} M).

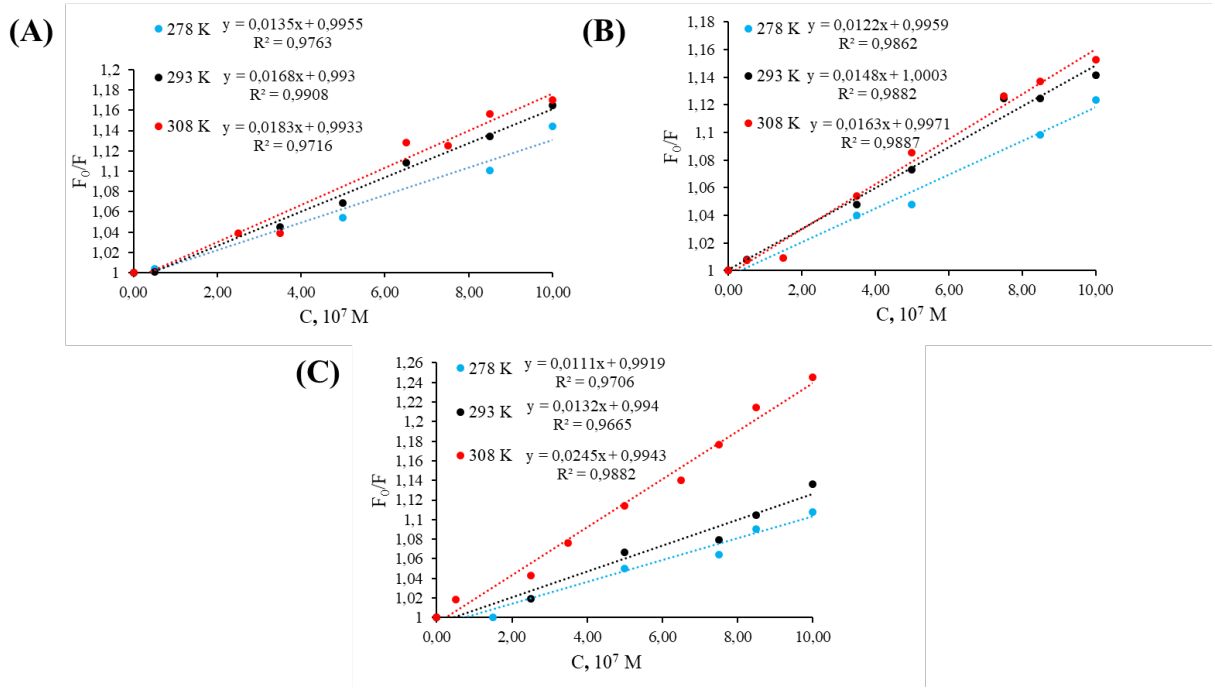

Figure S33. The graphs are plotted in the linearization of Stern–Volmer coordinates for the systems **4** + BSA (A), **5** + BSA (B), and **6** + BSA (C).

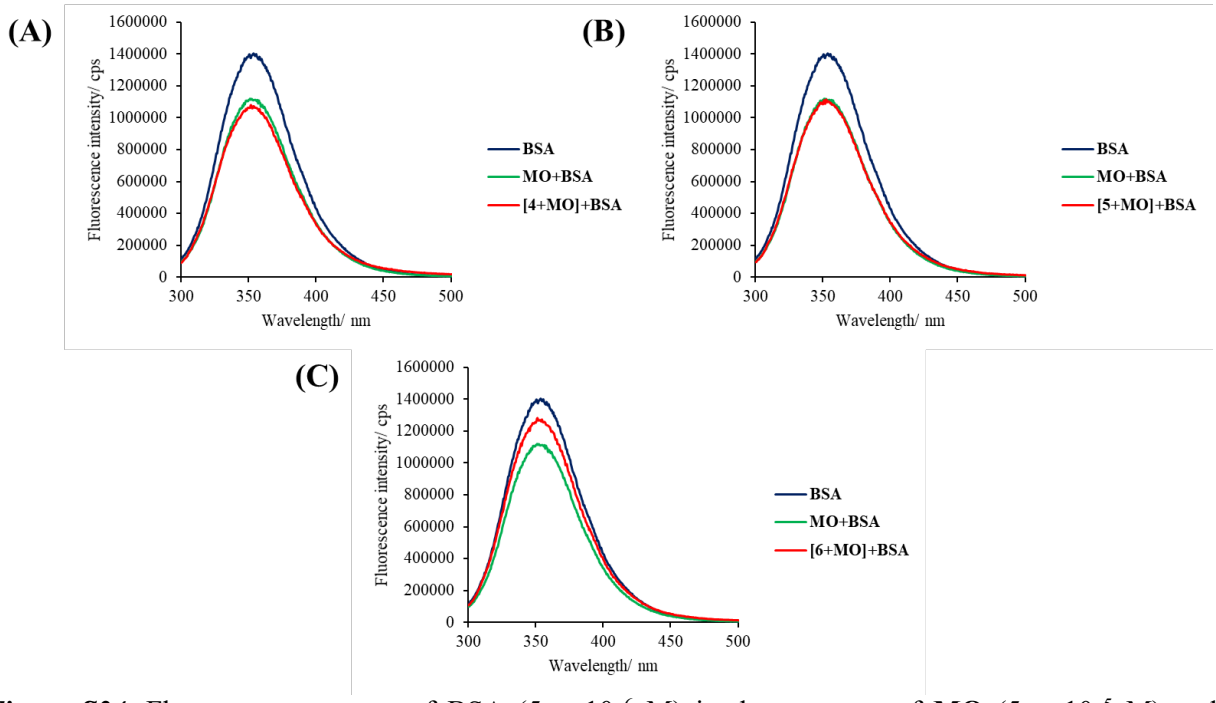

Figure S34. Fluorescence spectra of BSA (5×10^{-6} M) in the presence of **MO** (5×10^{-5} M) and equimolar systems [**4–MO**] (A), [**5–MO**] (B), and [**6–MO**] (C) (5×10^{-5} M).

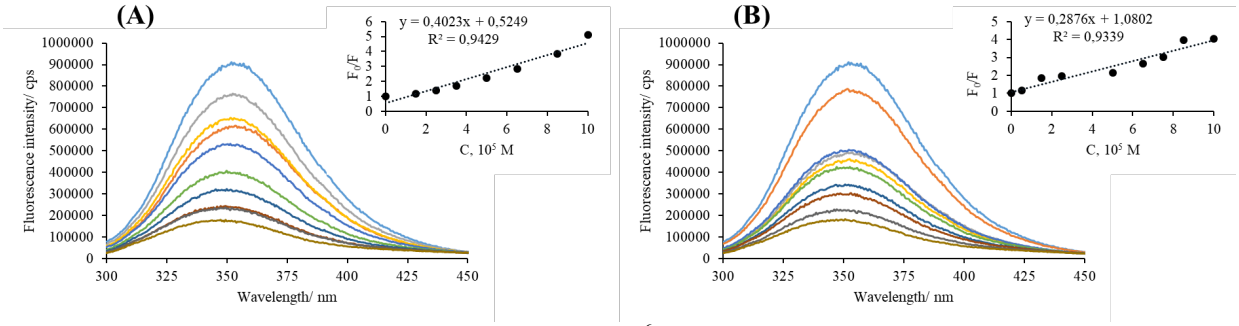

Figure S35. Fluorescence spectra of BSA (5×10^{-6} M) at different (A) [**4–MO**] and (B) [**5–MO**] concentrations (5×10^{-6} – 1×10^{-4} M); the graph plotted in the linearization of Stern–Volmer coordinates for corresponding systems [**4–MO**]+BSA and [**5–MO**]+BSA.

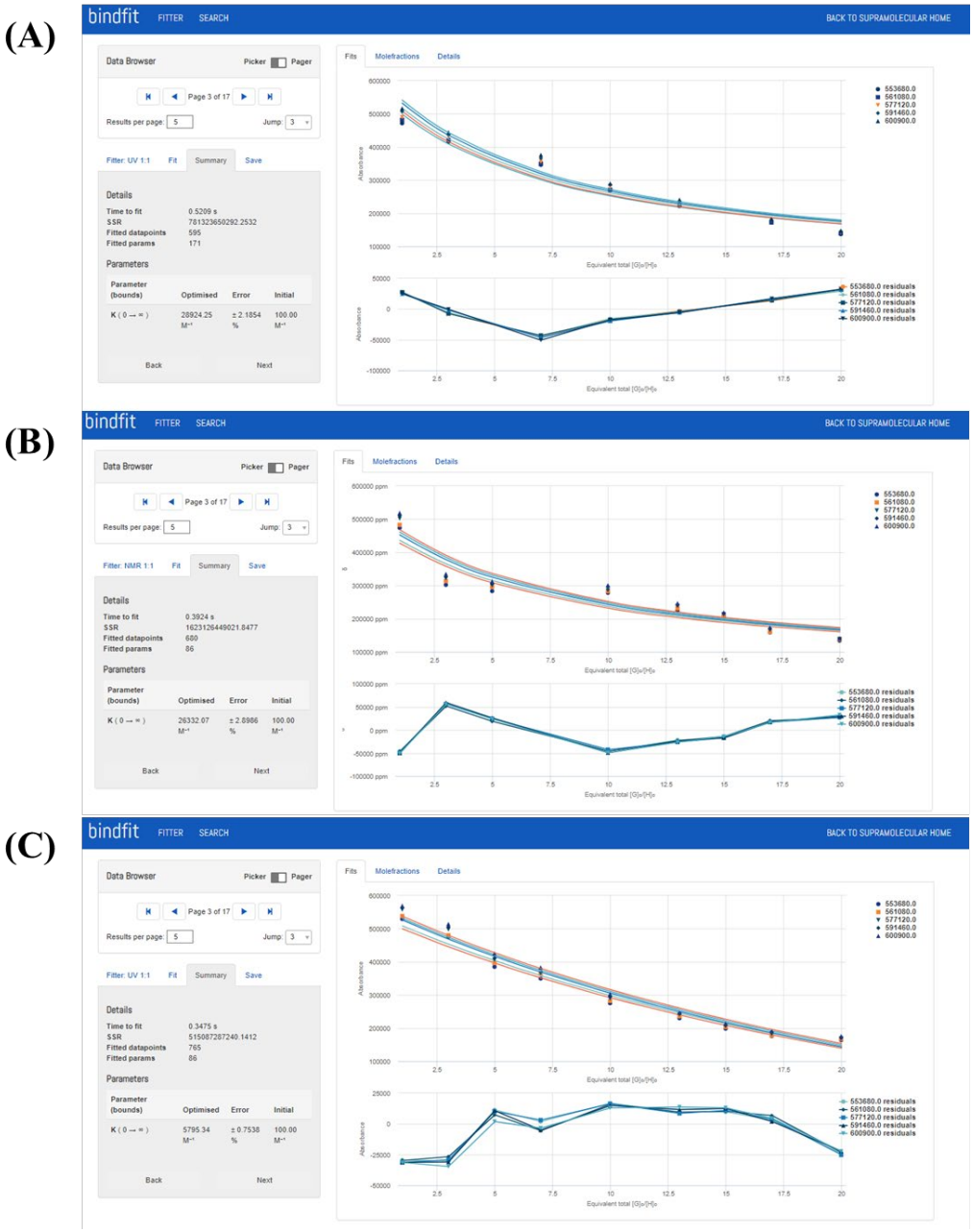

Figure S36. Bindfit screenshots taken from the summary window of the website supramolecular.org. This screenshots shows the raw data for fluorescent titration of (A) [**4–MO**]+BSA, (B) [**5–MO**]+BSA, (C) [**6–MO**]+BSA in phosphate buffer at pH = 7.4, the data fitted to 1:1 binding model.

Table S2. The aggregate sizes (hydrodynamic particle diameters d, nm), intensity distribution of particles formed as a result of self–assembly of BSA with pillar[5]arenes **4-6** (1:1) in a phosphate buffer solution (pH = 7.4), polydispersity index (PDI), content of monomeric protein form (%).

System	**PDI**	**d, nm**	**Content of albumin monomeric form (%)**
BSA	0.13±0.02	9±0	98
4+BSA	0.26±0.03	9±0	94
5+BSA	0.21±0.03	9±0	93
6+BSA	0.23±0.02	9±0	90

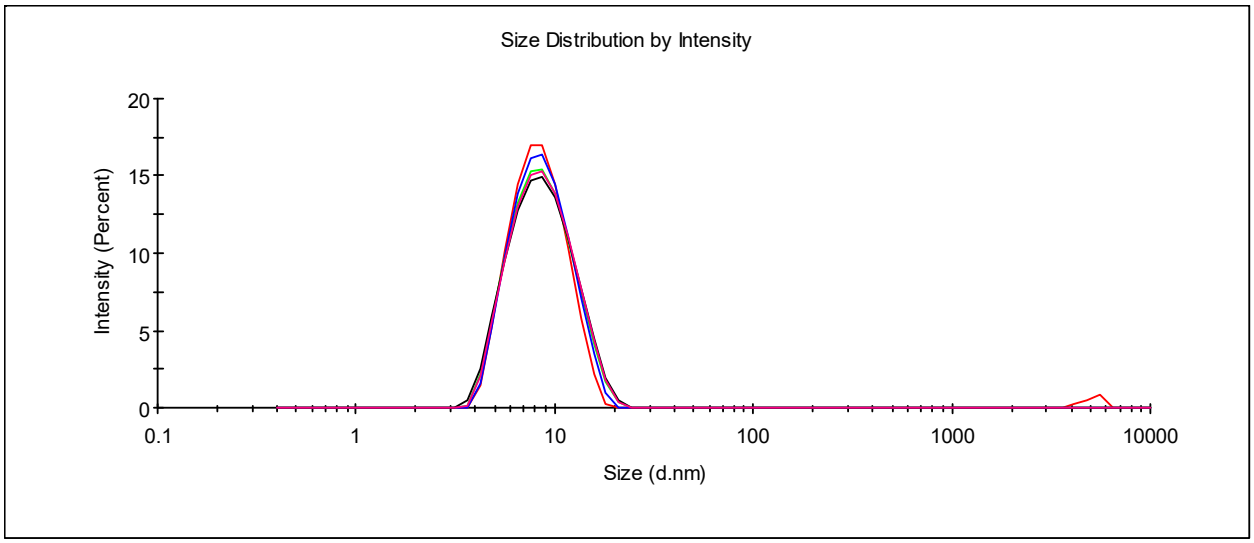

Figure S37. Size distribution of associates formed by BSA in a phosphate buffer solution (pH = 7.4) (1×10^{-4} M).

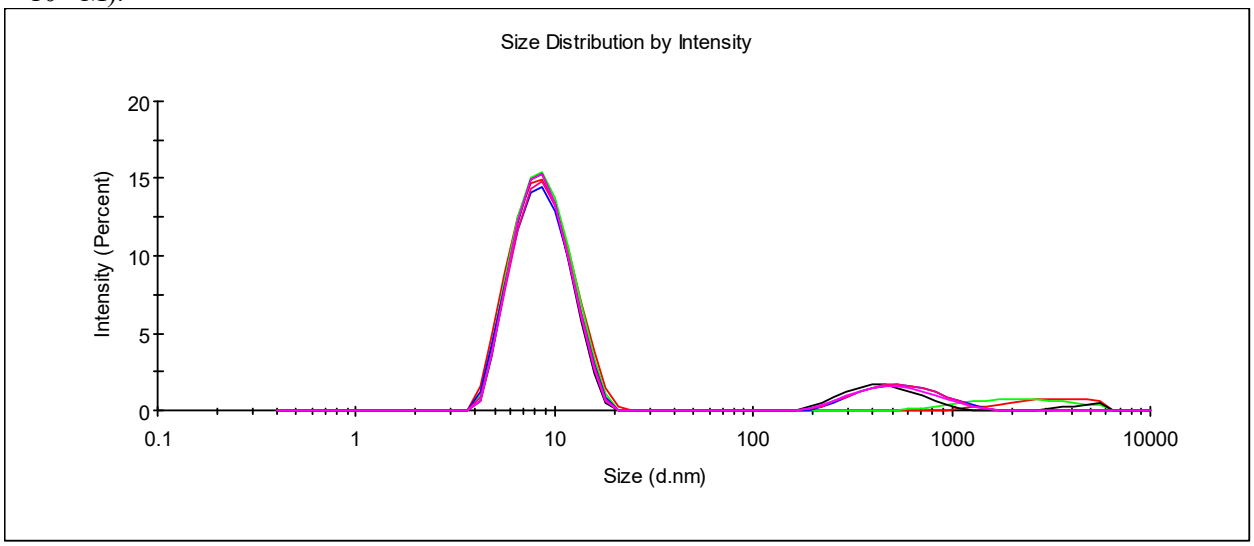

Figure S38. Size distribution of associates formed by BSA and **4** (1:1) in a phosphate buffer solution (pH = 7.4) (1×10^{-4} M).

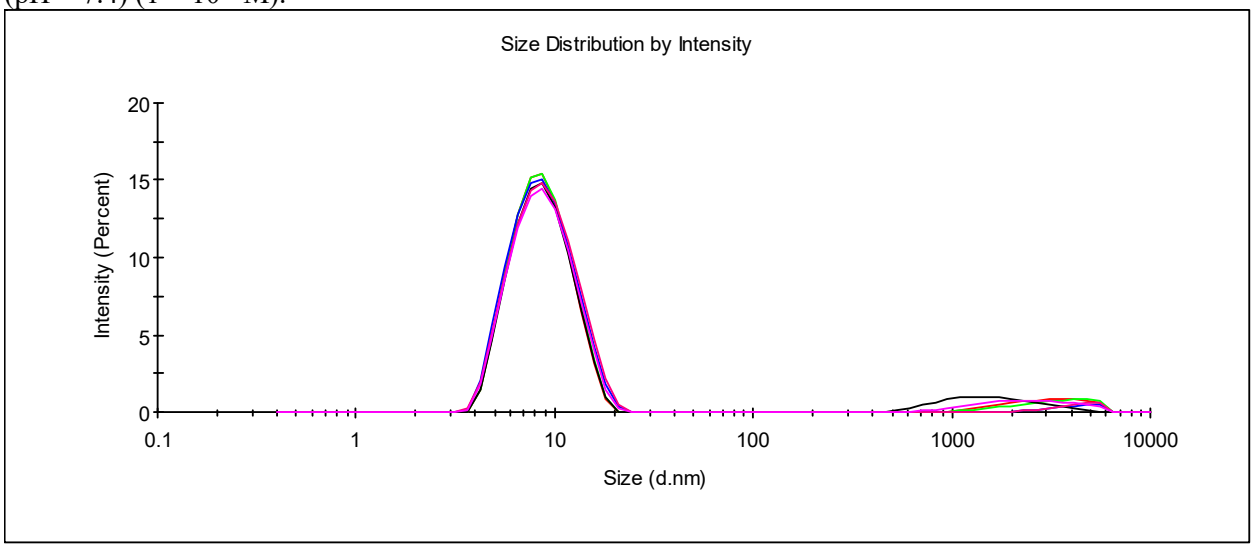

Figure S39. Size distribution of associates formed by BSA and **5** (1:1) in a phosphate buffer solution (pH = 7.4) (1×10^{-4} M).

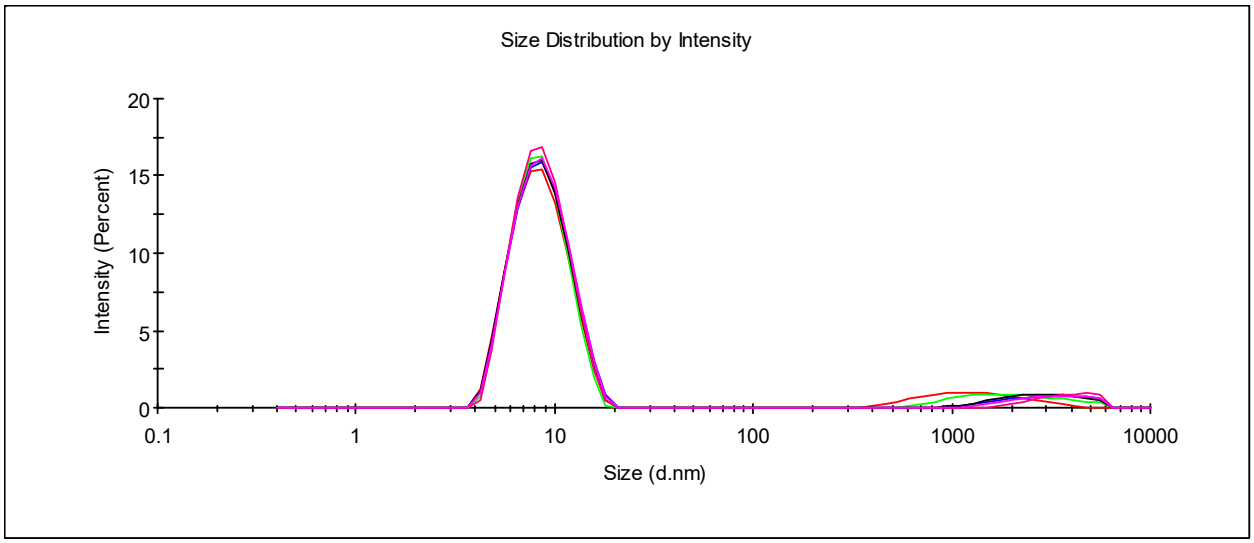

Figure S40. Size distribution of associates formed by BSA and **6** (1:1) in a phosphate buffer solution (pH = 7.4) (1×10^{-4} M).

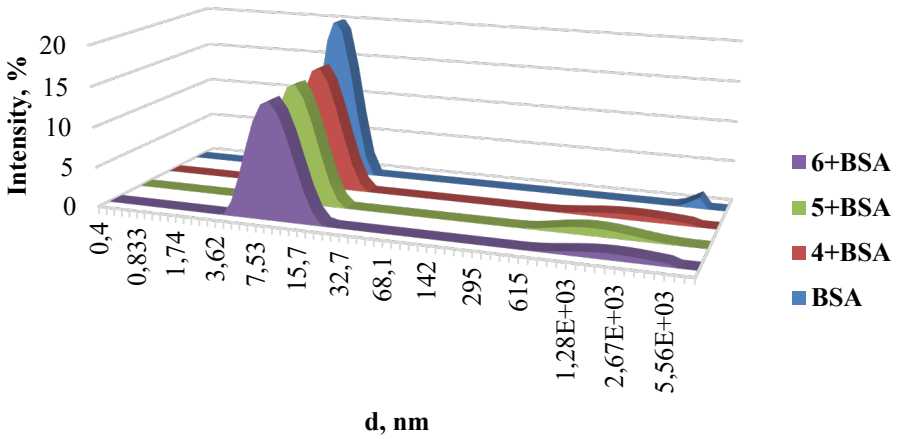

Figure S41. DLS profiles of solutions of BSA in the presence of the macrocycles **4-6**.

Table S3. The aggregate sizes (hydrodynamic particle diameters d, nm), intensity distribution of particles formed as a result of self–assembly of BSA with pillar[5]arenes **4-6**–**MO** blocks (1:1) in a phosphate buffer solution (pH = 7.4), polydispersity index (PDI), content of monomeric protein form (%).

System	PDI	d, nm	Content of albumin monomeric form (%)
[**4–MO**]+BSA	0.31±0.01	9±0	88
[**5–MO**]+BSA	0.33±0.02	10±0	85
[**6–MO**]+BSA	0.31±0.05	10±0	81

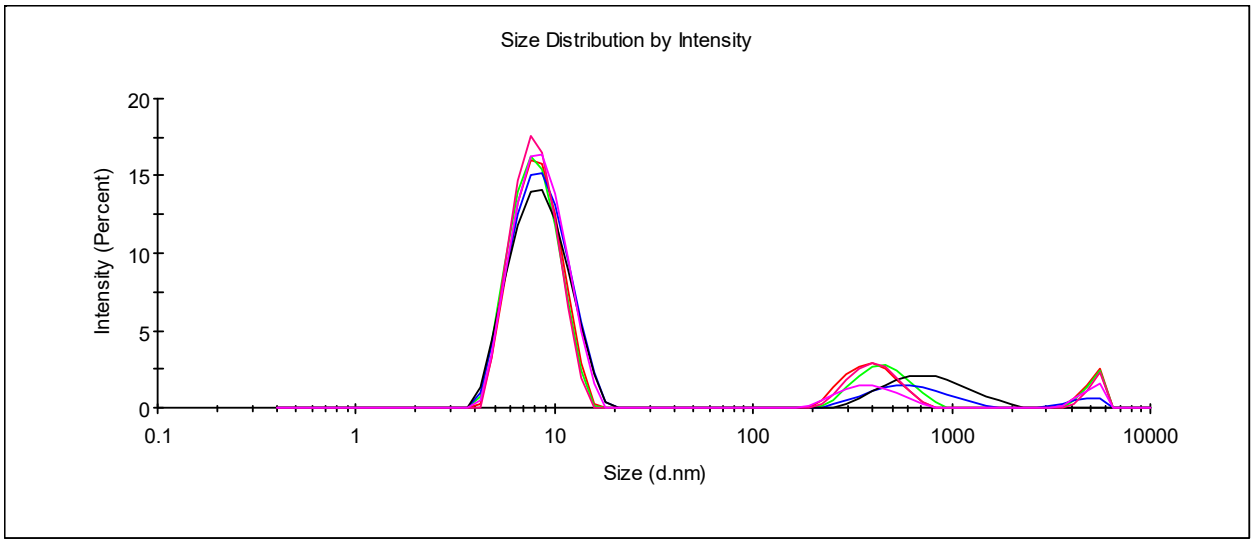

Figure S42. Size distribution of associates formed by [**4–MO**]+BSA (1:1) in a phosphate buffer solution (pH = 7.4) (1×10^{-4} M).

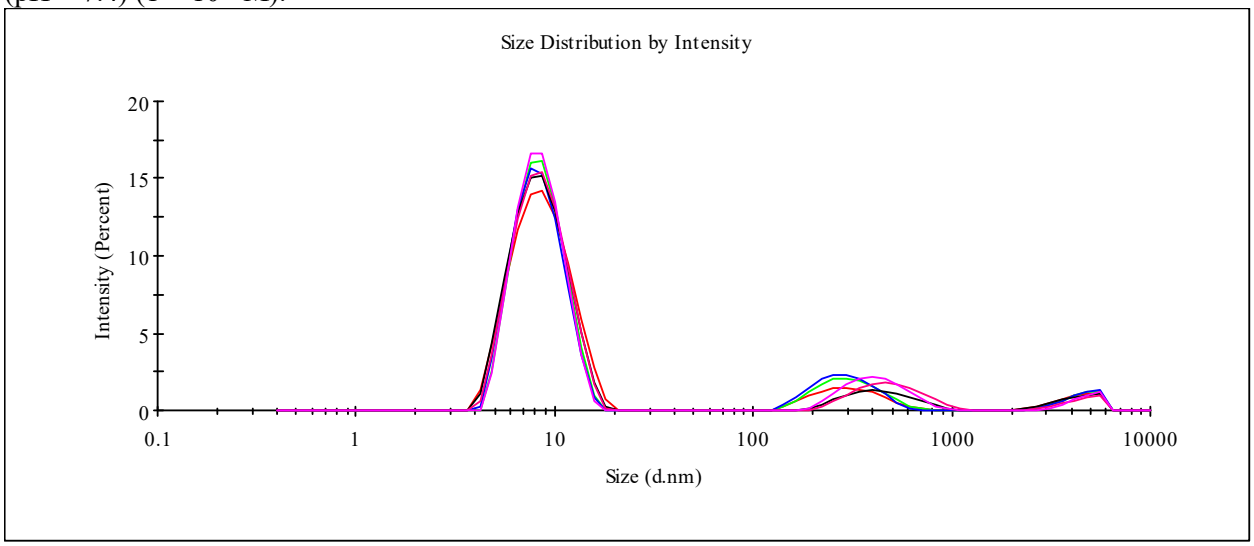

Figure S43. Size distribution of associates formed by [**5–MO**]+BSA (1:1) in a phosphate buffer solution (pH = 7.4) (1×10^{-4} M).

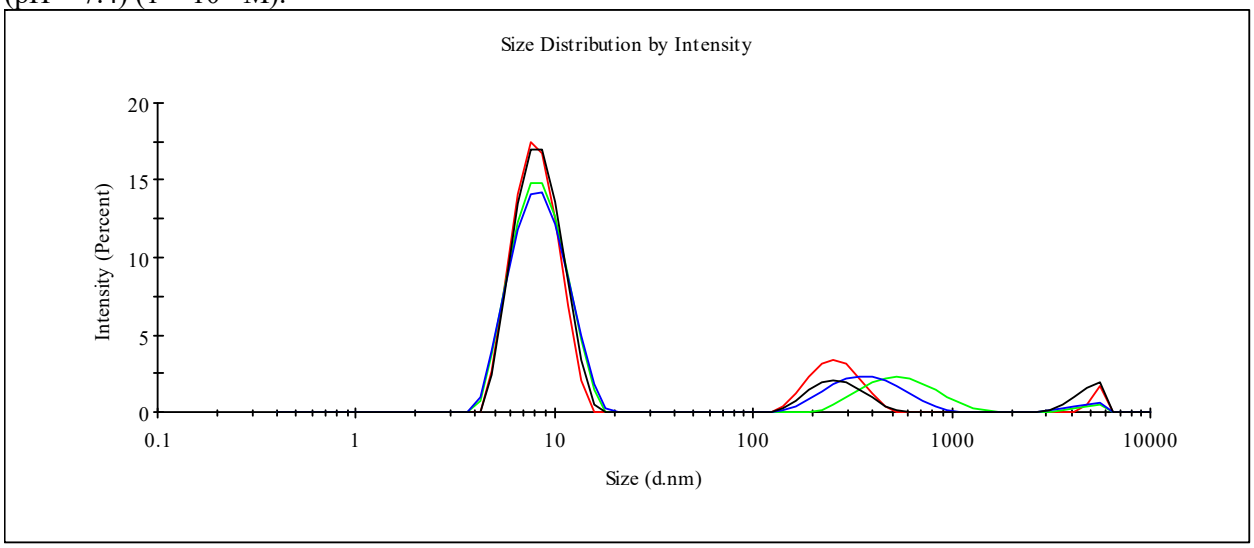

Figure S44. Size distribution of associates formed by [**6–MO**]+BSA (1:1) in a phosphate buffer solution (pH = 7.4) (1×10^{-4} M).

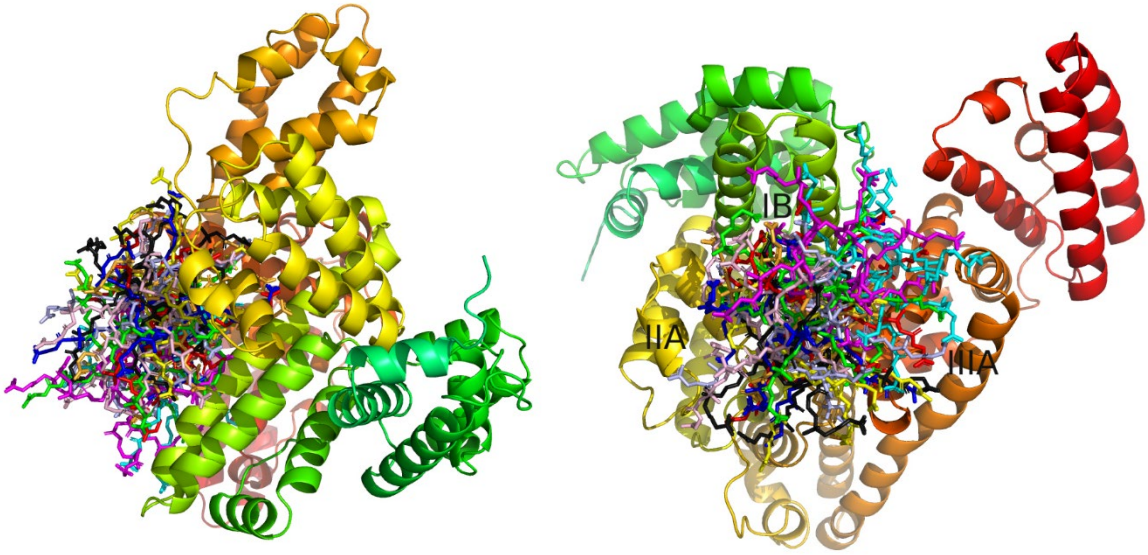

Figure S45. Poses of **5** from 10 top scoring runs of docking to BSA. Two projections are shown, neighboring BSA domains are labeled in the right picture.

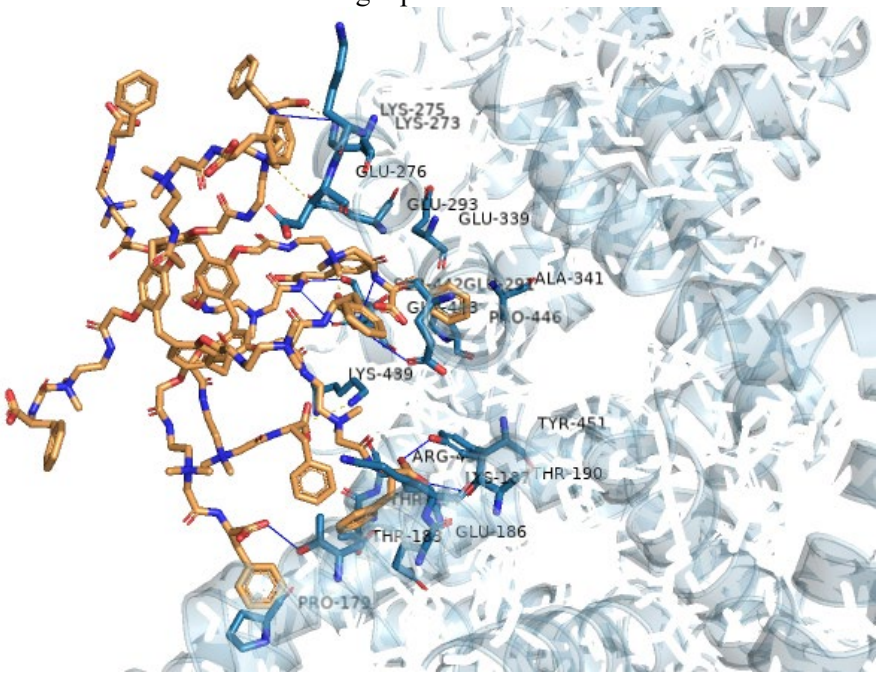

Figure S46. Top scoring poses of **4** and its contacts with BSA residues.

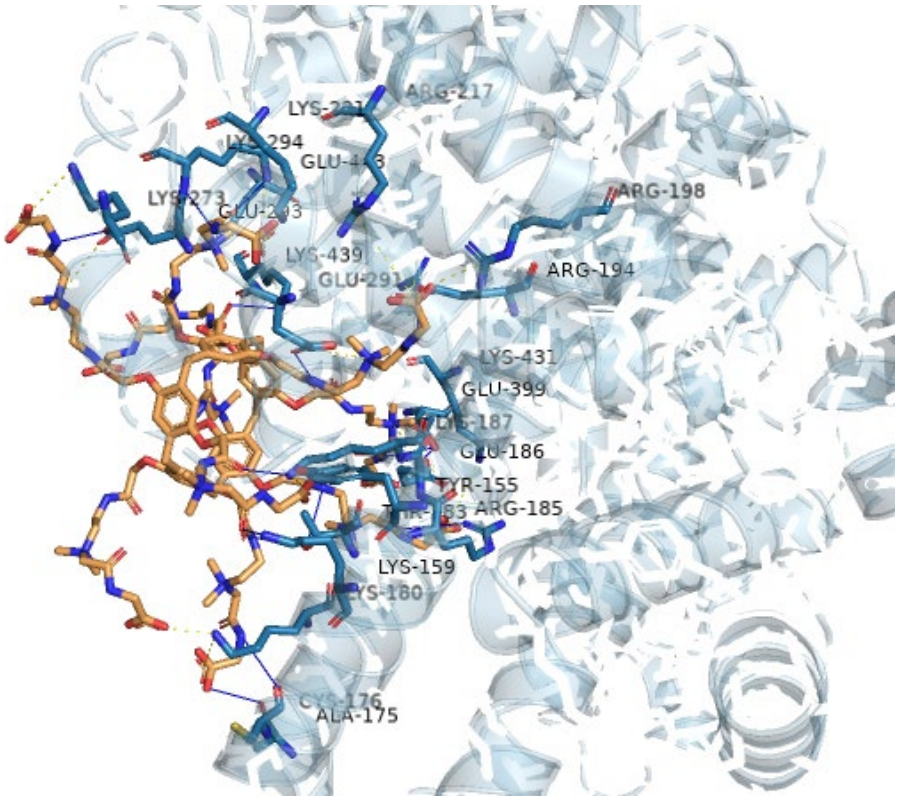

Figure S47. Top scoring poses of **5** and its contacts with BSA residues.

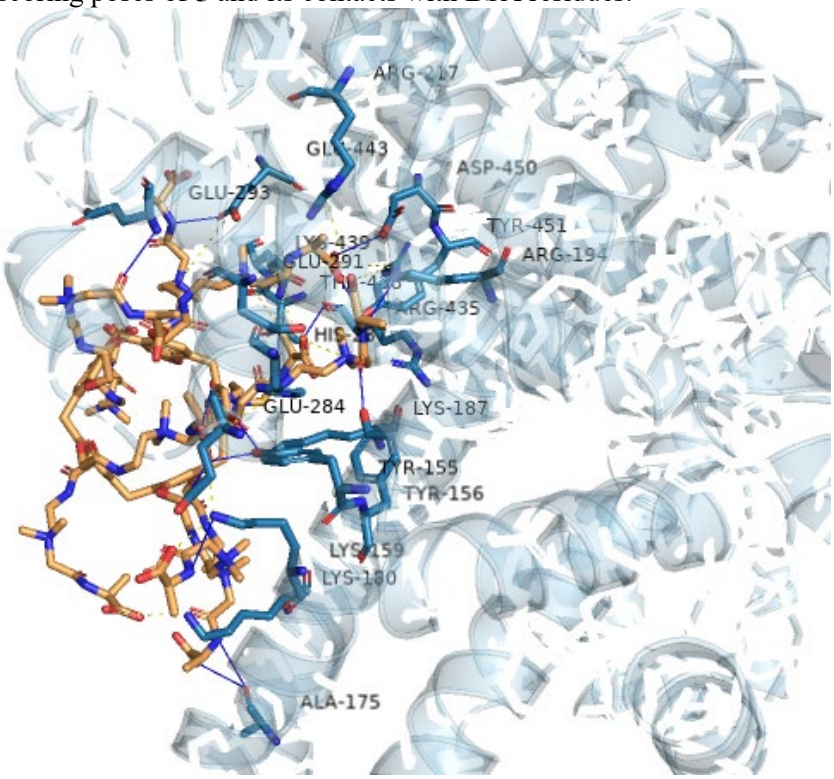

Figure S48. Top scoring poses of **6** and its contacts with BSA residues.

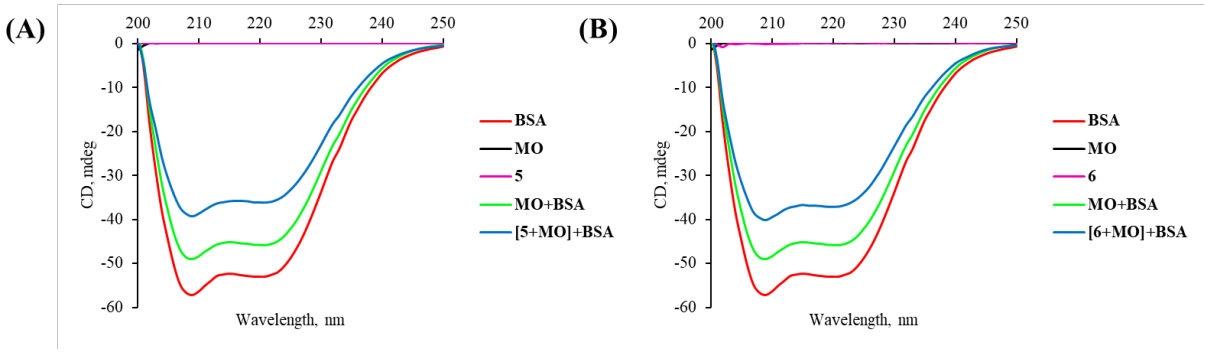

Figure S49. CD spectra of mixtures (A) [**5–MO**]+BSA; (B) [**6–MO**]+BSA in phosphate buffer solution at pH = 7.4 (5×10^{-7} M).

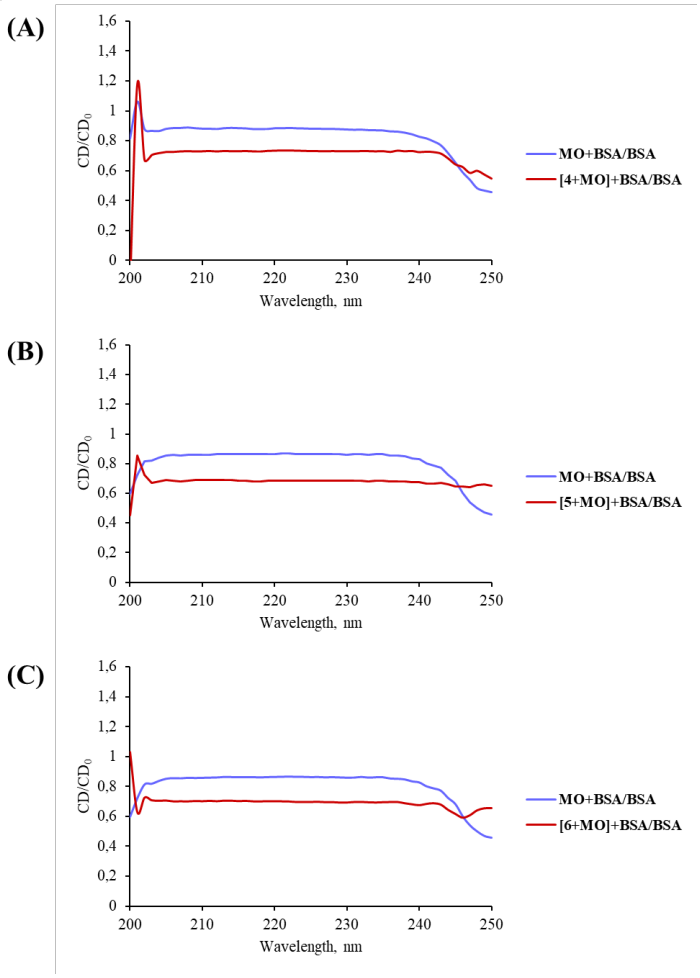

Figure S50. Graphs of the ratio of the circular dichroism signals of mixtures and BSA ellipticity to the wavelength for the (A) [**4–MO**]+BSA, (B) [**5–MO**]+BSA, and (C) [**6–MO**]+BSA

5. Supplemental References

[S1] Sultanaev, V., Yakimova, L., Nazarova, A., Mostovaya, O., Sedov, I., Davletshin, D., Gilyazova, E., Bulatov, E., Li, Z.-T., Zhang, D.-W., Stoikov, I. (2023). Decasubstituted Pillar[5]arene Derivatives Containing *L*–Tryptophan and *L*–Phenylalanine Residues: Non-Covalent Binding and Release of Fluorescein from Nanoparticles. Int. J. Mol. Sci. *24, 7700*.

[S2] Nazarova A.A., Sultanaev, V.R., Yakimova, L.S., Stoikov, I.I. (2022). Synthesis and Supramolecular Properties of Water-soluble Pillar[5]arenes Containing Amino Acid Residues. Russ. J. Org. Chem. *58(8), 1115–1122*.

[S3] Joosten, R.P., Long, F., Murshudov, G.N., Perrakis, A. (2014). The PDB_REDO server for macromolecular structure model optimization. IUCrJ. *1(4), 213–220*.

[S4] Sedov, I., Nikiforova, A., Khaibrakhmanova, D. (2020). Evaluation of the binding properties of drugs to albumin from DSC thermograms. International journal of pharmaceutics. *583, 119362*.